UNCLASSIFIED

Security Classification

AD 740617

DOCUMENT CONTROL DATA - R & D

(Security classification of title, body of abstract and indexing annotation must be entered when the overall report is classified)

1. ORIGINATING ACTIVITY (Corporate author) The Ohio State University Research Foundation, ElectroScience Laboratory 1320 Kinnear Road, Columbus, Ohio 43212	2a. REPORT SECURITY CLASSIFICATION UNCLASSIFIED 2b. GROUP N/A

3. REPORT TITLE

IMPERFECT DIFFERENTIAL DETECTION OF A BIPHASE MODULATED SIGNAL - AN EXPERIMENTAL AND ANALYTICAL STUDY

4. DESCRIPTIVE NOTES (Type of report and inclusive dates)

Technical Report

5. AUTHOR(S) (First name, middle initial, last name)

Thomas W. Miller

6. REPORT DATE	7a. TOTAL NO. OF PAGES	7b. NO. OF REFS
February 1972	98	14

8a. CONTRACT OR GRANT NO.	9a. ORIGINATOR'S REPORT NUMBER(S)
F30602-69-C-0112 Job Order No. 45190000	OSURF 2738-5
	9b. OTHER REPORT NO(S) (Any other numbers that may be assigned this report) RADC-TR-72-16

10. DISTRIBUTION STATEMENT

Approved for public release; distribution unlimited.

11. SUPPLEMENTARY NOTES	12. SPONSORING MILITARY ACTIVITY
None	Rome Air Development Center (CORC) Griffiss Air Force Base, New York 13440

13. ABSTRACT

The results of an experimental investigation of the effects of bit synchronization error and carrier frequency uncertainty on the performance of receivers used to demodulate differential phase shift keyed (DPSK) signals are presented. Also, previous analytical results relating to the differential detector (DD) are summarized and an expression for the performance of the perfectly timed DD with frequency uncertainty is derived. The bit error probability and the probability of two consecutive errors are used as performance measures. The experimental and analytical results obtained apply to cases in which the carrier is biphase modulated with the differentially encoded bit stream, the (equivalent) noise at the receiver input is white and Gaussian distributed, the bit synchronization error is Gaussian distributed, and the error in the carrier frequency estimate is constant as a function of time. The results presented provide a basis for the design of systems employing DPSK and differential detection when changing system geometries must be considered, e.g., in satellite communications systems.

DD FORM 1 NOV 68 1473

UNCLASSIFIED

Security Classification

14 KEY WORDS	LINK A		LINK B		LINK C	
	ROLE	WT	ROLE	WT	ROLE	WT
Differential phase shift keying						
Differential detection						
Bit synchronization error						
Frequency uncerteinty						
Consecutive errors						
Analyses						
Instrumentation						
Experimental results						

IMPERFECT DIFFERENTIAL DETECTION OF A BIPHASE MODULATED SIGNAL - AN EXPERIMENTAL AND ANALYTICAL STUDY

Thomas W. Miller

The Ohio State University Research Foundation

FOREWORD

This report, OSURF number 2738-5, was prepared at the Electro-Science Laboratory, Department of Electrical Engineering, The Ohio State University, Columbus, Ohio. Research was conducted under contract F30602-69-C-0112, Job Order Number 45190000, for Rome Air Development Center, Griffiss Air Force Base, New York. Mr. John J. Patti (CORC) was the RADC Project Engineer.

The material contained in this report was also submitted to the Department of Electrical Engineering, The Ohio State University, in partial fulfillment of the requirements for the Master of Science degree.

The author wishes to express his appreciation to Dr. Ronald J. Huff for contributing many valuable ideas and comments throughout the writing of this report and during the preceding research work and to Dr. Robert B. Lackey for his guidance and counseling. Special thanks are also due Messrs. Robert C. Taylor and Daniel C. Upp for help and encouragement.

This report has been reviewed by the Information Office (OI) and is releasable to the National Technical Information Service (NTIS).

This technical report has been reviewed and is approved.

Approved: JOHN J. PATTI
Project Engineer

Approved: JAMES E. McFEE, Chief
Communications Techniques Branch
Communications & Navigation Division

ABSTRACT

The results of an experimental investigation of the effects of bit synchronization error and carrier frequency uncertainty on the performance of receivers used to demodulate differential phase shift keyed (DPSK) signals are presented. Also, previous analytical results relating to the differential detector (DD) are summarized and an expression for the performance of the perfectly timed DD with frequency uncertainty is derived. The bit error probability and the probability of two consecutive errors are used as performance measures. The experimental and analytical results obtained apply to cases in which the carrier is biphase modulated with the differentially encoded bit stream, the (equivalent) noise at the receiver input is white and Gaussian distributed, the bit synchronization error is Gaussian distributed, and the error in the carrier frequency estimate is constant as a function of time. The results presented provide a basis for the design of systems employing DPSK and differential detection when changing system geometries must be considered, e.g., in satellite communications systems.

TABLE OF CONTENTS

TABLE OF CONTENTS (Cont.)

CHAPTER I
INTRODUCTION

The combination of differential phase shift keying (DPSK) and differential detection is known to provide optimum performance in digital communications systems which employ a carrier signal when an a priori estimate of the carrier phase is not available at the receiver. However, to date, DPSK (and differential detection) has not been utilized extensively in conventional space communications and telemetry systems because an accurate estimate of the carrier phase can usually be established and continuously maintained at the receiver. As a result, phase shift keying (PSK) and (partially) coherent detection usually provide best performance. Recently, considerable interest has developed in non-conventional systems in which pulsed-envelope signals are employed to convey digital information, e.g., time division multiple access (TDMA) space communications systems[1-3]. In such systems, it is often either impossible or impractical to retain phase information accurately from pulse to pulse. On assuming that phase information would have to be acquired at the beginning of each pulse, that the bit timing information required to identify each signalling interval can be retained from pulse to pulse, and that fewer than approximately one thousand data bits are to be conveyed per pulse, DPSK and

differential detection can provide better overall performance than PSK and (partially) coherent detection. Differential detection is markedly superior to partially coherent detection in TDMA systems when only a few tens of bits are transmitted per pulse and the assumptions just stated are applicable[5]. Thus, there is a need for detailed information regarding the design and performance of practical differential detectors.

The purposes of this report are threefold: 1) to summarize the available analytical results relating to differential detection, 2) to extend available analytical results by determining the effects of an error in the carrier frequency estimate on the performance of the differential detector (DD), and 3) to present extensive experimental results describing the performance of a practical, i.e., imperfect, DD when the channel is Gaussian. The experimental results verify the accuracy of four theoretical results: 1) the results relating the bit error probability, P_E, to the bit energy to single-sided noise density ratio, E_b/N_o, when the DD is ideally implemented[6-9], 2) the results obtained by Salz and Saltzberg[11] which show the probability of two consecutive errors as a function of E_b/N_o when the DD is ideally implemented, 3) the results derived by Huff[1] relating P_E to E_b/N_o when the DD is imperfectly timed, and 4) the analytical results to be derived which show the effects of an error in the estimate of the carrier

frequency on P_E when the DD is otherwise ideally instrumented.* Experimental results are also given which show the combined effects of bit timing error and an error in the carrier frequency estimate on P_E and on the probability of two consecutive errors, for which no corresponding theoretical results are available. All results apply when biphase modulation is employed, and when the channel simply attenuates and delays the transmitted signal, the receiver bandwidth is much larger than the signalling rate, and the (equivalent) noise at the receiver input is white and Gaussian distributed.

---

*The effect of frequency offset on differential detection has been determined independently by Henry[10]. The different approaches employed in the two analyses lead to expressions for P_E which differ considerably in form. However, spot checks of the numerical results obtained using the two expressions indicate that they are equivalent.

CHAPTER II
A DESCRIPTION OF THE DIFFERENTIAL DETECTOR AND A SUMMARY OF AVAILABLE ANALYTICAL RESULTS

A. Introduction

In this section, analytical results applicable to differential detection are summarized. This summary is preceded by a description of the signalling waveform and methods for differentially detecting the data carrying signal in the presence of noise. Notations, assumptions, and discussions applicable to subsequent analyses are given.

B. System Description

In systems employing (antipodal) DPSK, the carrier signal is biphase modulated with a differentially encoded bit stream. Either of two coding conventions can be used to generate the modulation waveform from the data bit stream. To be specific, it is assumed that a "0" in the data bit stream is encoded as (0, 0) or (1, 1), i.e., the encoded bit in the current interval is the same as the encoded bit in the previous interval. Correspondingly, a "1" in the data bit stream is encoded as (0, 1) or (1, 0). This encoding convention is illustrated by example in Fig. 1. Note that the first signalling interval is devoted to

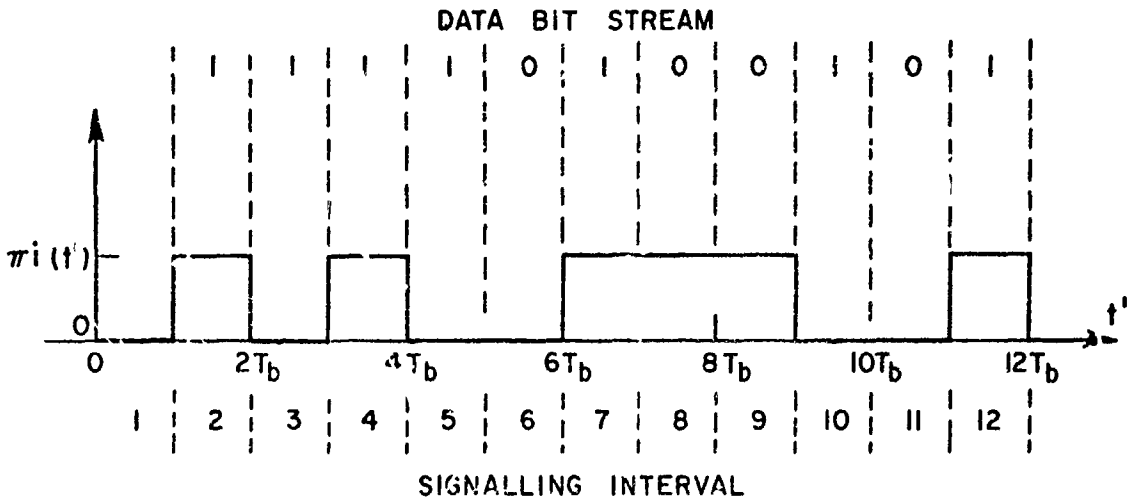

Fig. 1. A differential encoding example.

establishing a reference, so that N + 1 intervals are required to transmit N information bits.

The transmitted waveform is assumed expressible as

$$(1) \qquad S_o(t') = A_o \cos[\omega_c t' + \pi i(t') + \alpha_o]$$

where i(t') represents the encoded bit stream and is constant at either 0 or 1 during a given bit interval. The amplitude A_o is assumed constant. At the demodulator's input, the message-carrying component of the received signal is assumed expressible in terms of the receiver time base as

$$(2) \qquad S(t) = \sqrt{2P_r} \cos[(\omega_c + \Delta\omega_c)t + \pi i(t - \epsilon) + \alpha]$$

where P_r represents the power in the received signal, ϵ represents the bit timing error, and $\Delta\omega_c/2\pi$ represents the doppler shift experienced by the transmitted signal. In general, $\Delta\omega_o$, ϵ, and α are time-varying quantities. An equivalent channel noise voltage, n(t), additively combines with S(t) at the receiver input to form the signal Z(t):

$$Z(t) = S(t) + n(t) \quad . \tag{3}$$

It is assumed that n(t) is a sample function from a zero mean white Gaussian process with an autocorrelation function given by

$$R_{nn}(\tau) = \frac{\delta(\tau)}{2} N_o \tag{4}$$

and a spectral density

$$S_{nn}(\omega) = \frac{N_o}{2} \quad -\infty < \omega < \infty \quad . \tag{5}$$

Additionally, the noise process n(t) is assumed to be ergodic.

A simplified block diagram of the differential detector (DD) to be investigated is shown in Fig. 2; an alternative detector configuration is shown in Fig. 3. Mathematically, the ideal integrate/dump differential detector (I/D DD) and the ideal matched filter/delay line differential detector (MF/DL DD) are identical. Although not proven rigorously, there is reason to believe that results to be presented for an

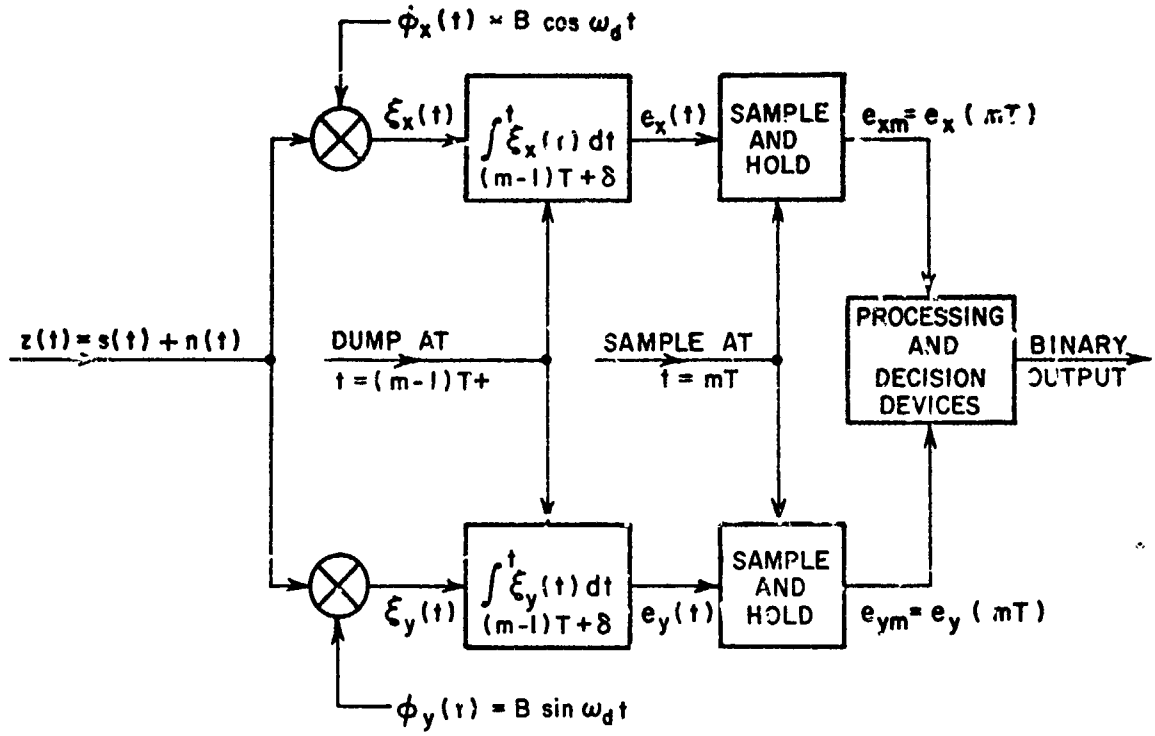

Fig. 2. A simplified block diagram of the differential detector to be investigated.

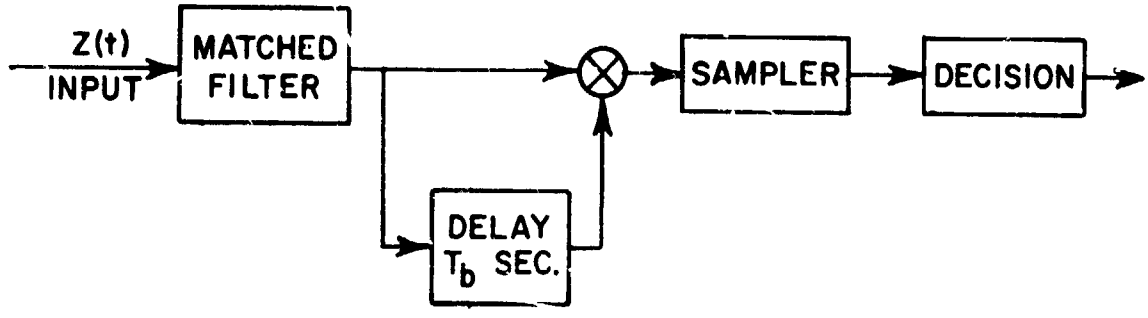

Fig. 3. A second possible implementation of the differential detector.

imperfect I/D differential detector apply when the same imperfections exist in a MF/DL DD[10]. Additional causes of performance degradation must be considered when a MF/DL DD is employed, e.g., intersymbol interference caused by imperfect filtering.

Referring to Fig. 2, the equivalent input signal Z(t) is first separated into (approximately) orthogonal components by multiplying it with two phase-quadrature sinusoids generated at the receiver. The resulting multiplier output waveforms, $\xi_x(t)$ and $\xi_y(t)$, contain both baseband and double frequency components. These waveforms are processed by integrate/dump circuits. Ideally, the integration intervals of length T_b seconds coincide with the intervals over which the phase of the received signal is constant. At the end of each bit interval, the integrator outputs are reset to zero. In practice, the integrate/dump commands are not precisely synchronized to the bit arrival time due to bit timing error. Additionally, practical integrators cannot be reset to zero instantaneously. The time required to reset (or dump) the integrator will be designated by δ: a positive constant.

At the end of the m-th integration interval, the integrator outputs are given by

$$e_{xm} = \int_{(m-1)T_b+\delta}^{mT_b} Z(t)\,\phi_x(t)\,dt = S_{xm} + n_{xm} \tag{6}$$

and

$$(7) \qquad e_{ym} = \int_{(m-1)T_b+\delta}^{mT_b} Z(t)\phi_y(t)\,dt = S_{ym} + n_{ym}$$

where

$$(8) \qquad S_{x,ym} = \int_{(m-1)T_b+\delta}^{mT_b} S(t)\phi_{x,y}(t)\,dt$$

and

$$(9) \qquad n_{x,ym} = \int_{(m-1)T_b+\delta}^{mT_b} n(t)\,\phi_{x,y}(t)\,dt \quad .$$

Using straightforward calculations, it can easily be shown that S_{xm} and S_{ym} are given by

$$(10) \qquad S_{xm} \doteq \frac{\sqrt{E_b}}{T_b} \int_{(m-1)T_b+\delta}^{mT_b} \cos[\pi i(t-\epsilon)]\,\cos(\Delta\omega_o t + \alpha - \gamma)\,dt$$

$$(11) \qquad S_{ym} \doteq -\frac{\sqrt{E_b}}{T_b} \int_{(m-1)T_b+\delta}^{mT_b} \cos[\pi i(t-\epsilon)]\,\sin(\Delta\omega_o t + o - \gamma)dt$$

when $\omega_d >>> \frac{2\pi}{T_b}$ and $\Delta\omega_o T_b < \frac{\pi}{2}$, the case of interest. In these expressions, ω_d is the radian frequency of the local oscillator* (LO), E_b is the energy per bit of the received signal, defined by

---

*In most systems, at least one down-converter is employed prior to detection. Thus the "carrier" frequency of the signal being detected, or, equivalently, the LO frequency, is actually an intermediate frequency (IF).

(12) $$E_b = P_r T_b$$

and γ represents the random phase of the LO. The radian frequency $\Delta\omega_o$ represents the error in the estimate of the carrier frequency (in radians per second), and is defined as

(13) $$\Delta\omega_o = \omega_c + \Delta\omega_c - \omega_d = 2\pi\Delta f_o$$

where Δf_o denotes the frequency offset. It will be assumed in subsequent discussion that Eqs. (10) and (11) are exact.

The noise components n_{xm} and n_{ym} are given by

(14) $$n_{xm} = \int_{(m-1)T_b+\delta}^{mT_b} n(t)\cos(\omega_d t + \gamma)dt$$

(15) $$n_{ym} = \int_{(m-1)T_b+\delta}^{mT_b} n(t)\sin(\omega_d t + \gamma)dt \quad .$$

The noise components are known to be independent, zero mean Gaussian processes having equal variances given by[3]

(16) $$\sigma^2 = \frac{N_o}{2}\left(\frac{T_b-\delta}{T_b}\right) \quad .$$

Voltages e_{xm} and e_{yrn} in Eqs. (6) and (7) (approximately) represent the components of $Z(t)$ in the orthogonal signal space $(\hat{\phi}_x, \hat{\phi}_y)$. The

signals present at the integrator outputs at time $t = mT_b$ can therefore be interpreted as the components of a vector $\overline{Z}_m$, where

$$\overline{Z}_m = e_{xm}\,\hat{\phi}_x + e_{ym}\,\hat{\phi}_y \quad . \tag{17}$$

Similarly, the message-carrying component can be interpreted as defining a signal vector $\overline{S}_m$:

$$\overline{S}_m = S_{xm}\,\hat{\phi}_x + S_{ym}\,\hat{\phi}_y \quad . \tag{18}$$

In differental detection, decisions are based on the dot product of the vectors $\overline{Z}_m$ and $\overline{Z}_{(m-1)}$. At the end of the m-th decision interval, the dot product V is given by

$$V = \overline{Z}_m \cdot \overline{Z}_{(m-1)} = |\overline{Z}_m|\,|\overline{Z}_{(m-1)}|\cos\phi \quad , \tag{19}$$

where ϕ is defined as the angle between $\overline{Z}_m$ and $\overline{Z}_{m-1}$. In terms of the integrator outputs at times $t_1 = (m-1)T_b$ and $t_2 = mT_b$, Eq. (19) reduces to

$$V = e_{xm}\,e_{x(m-1)} + e_{ym}\,e_{y(m-1)} \quad . \tag{20}$$

The value of V is compared to a threshold voltage in the decision circuitry. If the voltage V is greater than a threshold V_T, then the output of the threshold detector is a positive voltage; otherwise the output is zero. If the a priori probability of a "0" in the transmitted bit

stream is equal to one-half, it can be shown that the performance of the ideal differential detector is optimized by setting V_T equal to zero [6, 8]. For this case, the decision boundary is independent of the vector magnitudes. Formidable difficulties are encountered in attempting to determine the optimum decision rule when the DD is imperfectly timed and/or when an error exists in the carrier frequency estimate. However, even if the optimum decision rule were known, the decision rule applicable under ideal conditions would probably be employed to circumvent instrumentation difficulties. Thus, it is assumed that receiver decisions are based on the relations

$$e_{xm}e_{x(m-1)} + e_{ym}e_{y(m-1)} < 0 \quad \text{decide "1"} \tag{21}$$

and

$$e_{xm}e_{x(m-1)} + e_{ym}e_{y(m-1)} > 0 \quad \text{decide "0"} \tag{22}$$

In the absence of decision errors, the DD reproduces the data bit stream -- not the encoded bit stream -- at its output. Since the received signal is noisy, some receiver decisions will be in error. The probability that a given decision is in error, i.e., the bit error probability P_E, will be used as one measure of performance. The probability that two errors are made in succession, P_{E_D}, will be used as a second performance measure. Analytical results summarizing

the performance of an ideal DD are contained in the following section.

C. Ideal Differential Detection

1. The bit error probability

The bit error probability (BEP) of the ideally intrumented differential detector is given by [6-9]

$$P_E = \frac{1}{2} \exp[-E_b/N_o] \tag{23}$$

where E_b/N_o represents the bit energy to noise density ratio of the received waveform. As shown in Appendix A, the ideal DD performs nearly as well as the ideal coherent detector at high bit energy to noise density ratios. When the integrator dump time is non-zero, then the BEP of the otherwise ideally implemented DD is given by[1]

$$P_{E\delta} = \frac{1}{2} \exp\left[-\frac{P_r(T_b-\delta)}{N_o}\right] . \tag{24}$$

2. The probability of two consecutive errors

An analysis of the paired error probabilities of the ideal DD was performed by Salz and Saltzberg[11] which applies when the channel noise is a zero mean white Gaussian process. First, an expression for the probability of two consecutive errors, P_{E_D}, was found. This result was then divided by the bit error probability to obtain an

expression for the probability of error given that an error occurred in the previous bit interval;

$$(25) \qquad P_r(e_m | e_{(m-1)}) = \frac{P_{E_D}}{P_E} \quad .$$

In a form convenient for numerical evaluation, the expression for $P_r(e_m | e_{(m-1)})$ as a function of the bit energy to noise density ratio was found to be given by

$$(26) \qquad P_r(e_m | e_{(m-1)}) = \frac{1}{2\pi} \int_0^{\pi} a^2(\theta)[1 + \sqrt{M\pi} \cos\theta \exp(M^2 \cos^2\theta) b(\theta)] \, d\theta$$

where

$$(27) \qquad a(\theta) = \frac{2}{\sqrt{\pi}} \int_{M \cos\theta}^{\infty} \exp(-u^2) \, du$$

$$(28) \qquad b(\theta) = \frac{2}{\sqrt{\pi}} \int_{-M\cos\theta}^{\infty} \exp(-u^2) du$$

and

$$(29) \qquad M = \frac{E_b}{N_o} \quad .$$

The detection errors associated with non-adjacent symbols are independent when the DD is ideally instrumented. Thus, the conditional probability $P_r(e_m | e_{(m-n)})$ for $n \geq 2$ is approximately equal to the bit

error probability P_E. As a result, the occurrence of more than two consecutive errors is a relatively rare event.

The results of a numerical computation of Eq. (26) are given in Fig. 4. These results show that the ratio $P_r(e_m | e_{(m-1)})$ goes to zero as the bit energy to noise density ratio is increased without bound. This behavior is best explained by Masonson[4]: "An isolated single error can occur at very high signal to noise if two deviations are just large enough to differ by more than the half angle β, but not so large as to imply that another error will necessarily follow. For example, in differential binary systems, an error occurs if two deviations successively are -45° and -46°. In low noise, the next phase deviation is almost sure to be near zero and so a second error does not occur." This statement is further substantiated by the experimental results given in Section IV-C.

D. The Imperfectly Timed Differential Detector

The effect of bit timing error on the bit error probability of an otherwise ideal DD has been calculated by Huff[1]. Explicit numerical results were reported for the case where the timing error, ϵ, is Gaussian distributed with mean value $\bar{\epsilon}$ and standard deviation σ_ϵ. The loss mechanism when the timing error is non-zero will now be described and appropriate results summarized.

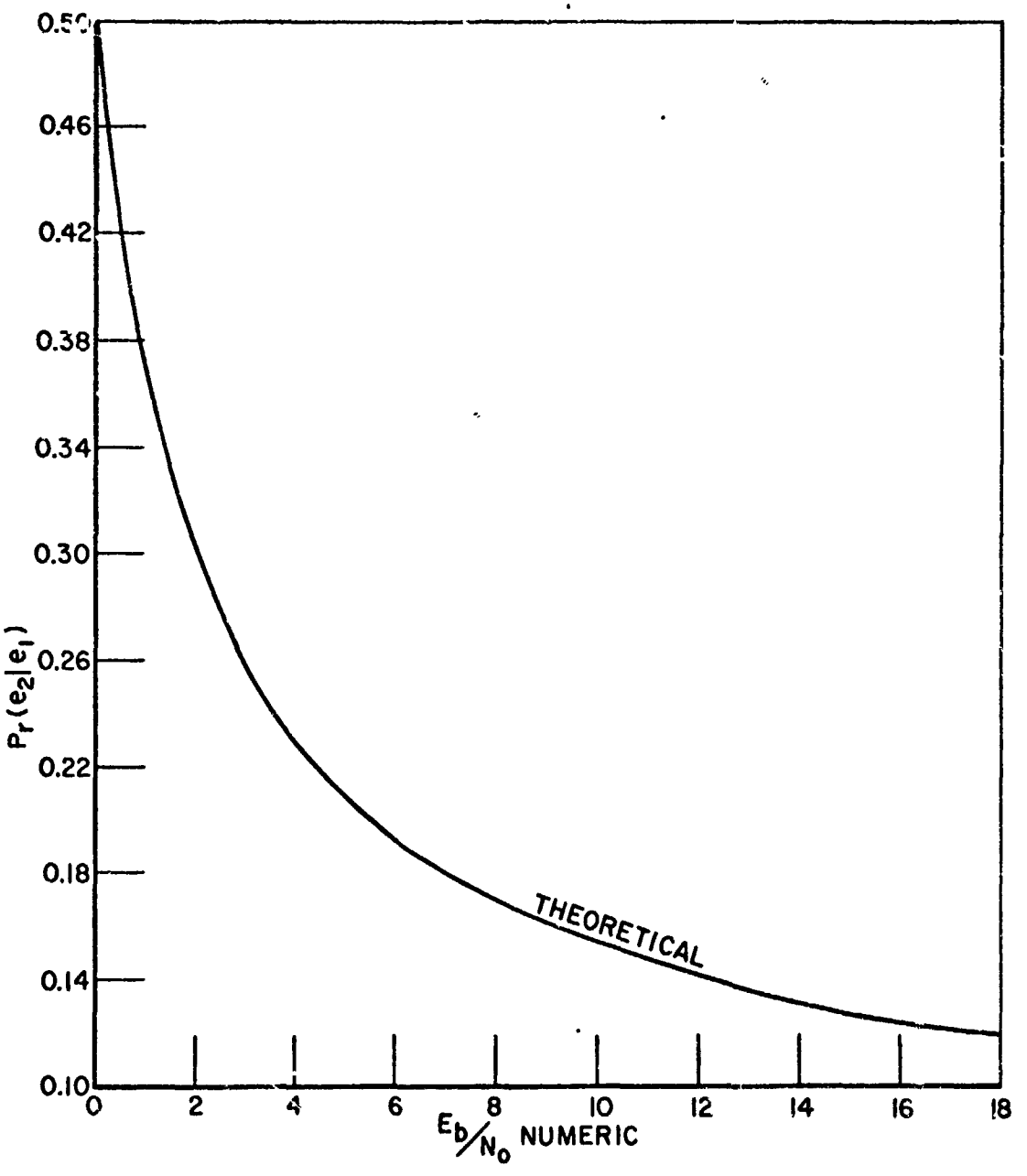

Fig. 4. The probability of error given that an error was detected in the previous bit interval versus the bit energy to noise density ratio for the ideally instrumented DD.

If it is assumed that the frequency offset and the integrator dump time are identically zero, and that $\beta=\alpha-\gamma$ changes only a few degrees during two consecutive bit intervals, then Eqs. (10) and (11) reduce to*

$$(30) \qquad S_{x1} = \frac{\sqrt{E_b}}{T_b} \int_0^{T_b} \cos[\pi i(t-\epsilon)]\, dt \cos\beta$$

$$(31) \qquad S_{y1} = \frac{\sqrt{E_b}}{T_b} \int_0^{T_b} \cos[\pi i(t-\epsilon)]\, dt \sin\beta$$

$$(32) \qquad S_{x2} = \frac{\sqrt{E_b}}{T_b} \int_{T_b}^{2T_b} \cos[\pi i(t-\epsilon)]\, dt \cos\beta$$

and

$$(33) \qquad S_{y2} = \frac{\sqrt{E_b}}{T_b} \int_{T_b}^{2T_b} \cos[\pi i(t-\epsilon)]\, dt \sin\beta \quad .$$

Correspondingly, $\bar{S}_1$ and $\bar{S}_2$ are given by

$$(34) \qquad \bar{S}_1 = \frac{\sqrt{E_b}}{T_b} \int_0^{T_b} \cos[\pi i(t-\epsilon)]\, dt \,[\cos\beta\, \hat{\phi}_x + \sin\beta\, \hat{\phi}_y]$$

and

---

*For convenience of notation, m is set equal to 1 with the understanding that each integral is performed over a bit interval that is interior to the transmitted bit stream.

$$(35) \qquad \bar{S}_2 = \frac{\sqrt{E_b}}{T_b} \int_{T_b}^{2T_b} \cos\left[\pi i(t-\epsilon)\right] dt \left[\cos\beta\,\hat{\phi}_x + \sin\beta\,\hat{\phi}_y\right] \quad .$$

In the absence of noise, the bit timing error affects the output of the integrator as shown in Fig. 5. This figure illustrates that the sample value S_{xm} depends on the bit sequence, the magnitude of ϵ, and the sign of ϵ. When a phase transition occurs in the received waveform during the m-th integration interval, the bit timing error causes a reduction in the magnitude of S_{xm}. Correspondingly, the signal to noise ratio at the integrator output is reduced since the statistics of the noise components $n_{x,ym}$ are independent of the timing error. When no transition occurs in the integration interval, the signal magnitude remains unaffected, provided the bit timing error does not exceed the bit length. Table 1 shows the effect of bit timing error on the magnitudes of the signal vectors $\bar{S}_1$ and $\bar{S}_2$, L_1 and L_2, for each of the sixteen possible four bit sequences $\{i_0, i_1, i_2, i_3\}$. As is evident from Table 1, the probability that an error is made in detecting the information conveyed by $|i_2 - i_1|$ depends on the bit timing error and the particular sequence $\{i_0, i_1, i_2, i_3\}$. Clearly, the probability of error when the data bit is a "1", P_1, is larger than the probability of error when the data bit is a "0", P_0, when the timing error is non-zero. This is a consequence of the fact that the signal phase experiences a transition between bits when a "1" occurs in the data bit stream. The

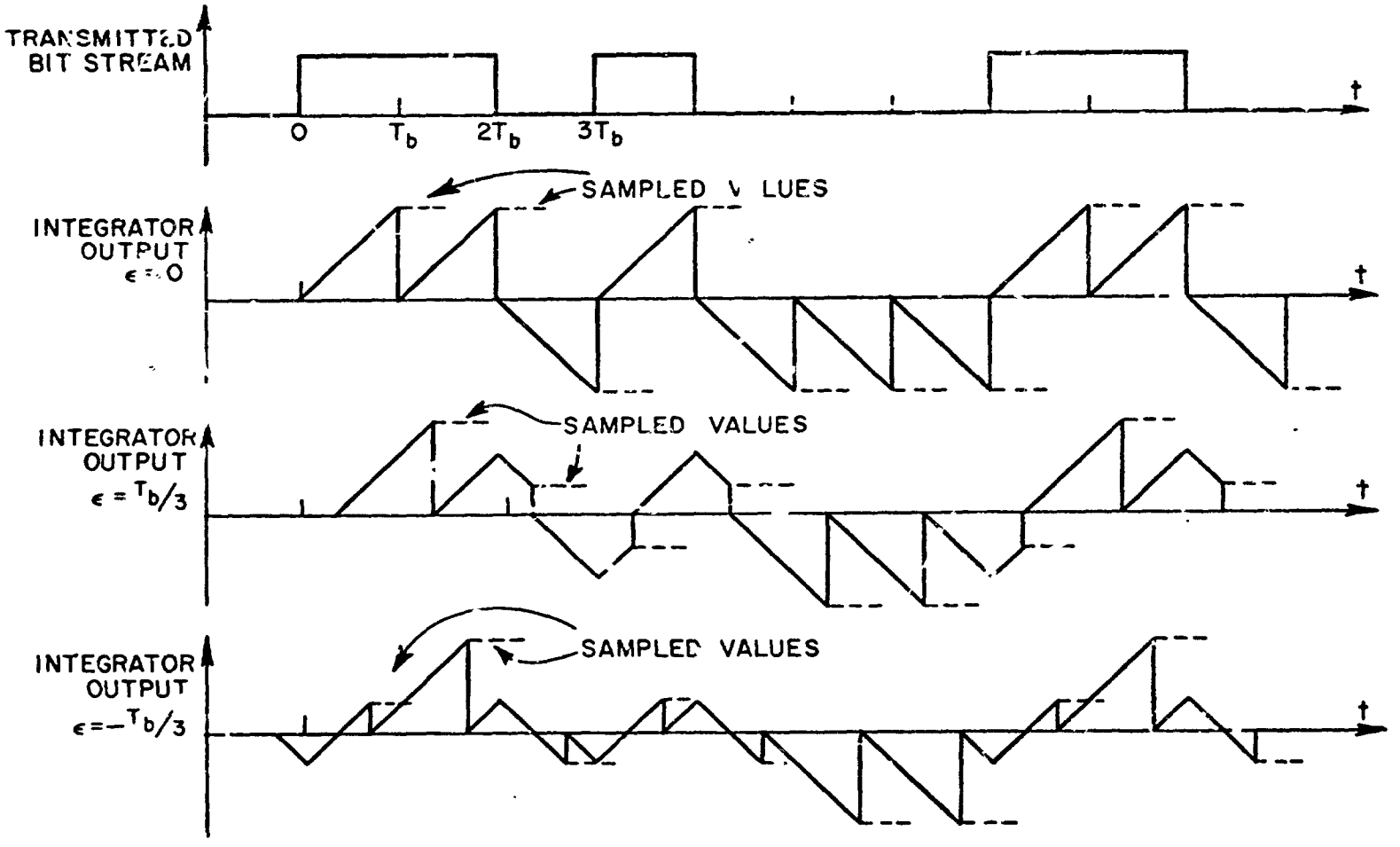

Fig. 5. An example illustrating the effects of bit timing error on the integrator's output assuming no channel noise is present.

TABLE 1
Summary of Signal-Vector Magnitude Relationships

Sequence Number	Sequence				Data Symbol	$T > \varepsilon > 0$		$-T < \varepsilon < 0$	
	i_0	i_1	i_2	i_3		$L_1/\sqrt{E_b}$	$L_2/\sqrt{E_b}$	$L_1/\sqrt{E_b}$	$L_2/\sqrt{E_b}$
1	0	0	0	0	0	1	1	1	1
2	0	0	0	1	0	1	1	1	$1-2\lvert\varepsilon\rvert/T$
3	1	0	0	0	0	$1-2\lvert\varepsilon\rvert/T$	1	1	1
4	1	0	0	1	0	$1-2\lvert\varepsilon\rvert/T$	1	1	$1-2\lvert\varepsilon\rvert/T$
5	1	1	1	1	0	1	1	1	1
6	1	1	1	0	0	1	1	1	$1-2\lvert\varepsilon\rvert/T$
7	0	1	1	1	0	$1-2\lvert\varepsilon\rvert/T$	1	1	1
8	0	1	1	0	0	$1-2\lvert\varepsilon\rvert/T$	1	1	$1-2\lvert\varepsilon\rvert/T$
9	0	0	1	0	1	1	$1-2\lvert\varepsilon\rvert/T$	$1-2\lvert\varepsilon\rvert/T$	$1-2\lvert\varepsilon\rvert/T$
10	0	0	1	1	1	1	$1-2\lvert\varepsilon\rvert/T$	$1-2\lvert\varepsilon\rvert/T$	1
11	1	0	1	0	1	$1-2\lvert\varepsilon\rvert/T$	$1-2\lvert\varepsilon\rvert/T$	$1-2\lvert\varepsilon\rvert/T$	$1-2\lvert\varepsilon\rvert/T$
12	1	0	1	1	1	$1-2\lvert\varepsilon\rvert/T$	$1-2\lvert\varepsilon\rvert/T$	$1-2\lvert\varepsilon\rvert/T$	1
13	1	1	0	1	1	1	$1-2\lvert\varepsilon\rvert/T$	$1-2\lvert\varepsilon\rvert/T$	$1-2\lvert\varepsilon\rvert/T$
14	1	1	0	0	1	1	$1-2\lvert\varepsilon\rvert/T$	$1-2\lvert\varepsilon\rvert/T$	1
15	0	1	0	1	1	$1-2\lvert\varepsilon\rvert/T$	$1-2\lvert\varepsilon\rvert/T$	$1-2\lvert\varepsilon\rvert/T$	$1-2\lvert\varepsilon\rvert/T$
16	0	1	0	0	1	$1-2\lvert\varepsilon\rvert/T$	$1-2\lvert\varepsilon\rvert/T$	$1-2\lvert\varepsilon\rvert/T$	1

average bit error probability, P_{E_ϵ}, depends on the relative frequency with which the sixteen possible four-bit sequences occur. Huff has shown that P_{E_ϵ} can be expressed as

$$(36) \qquad P_{E_\epsilon} = \frac{1}{\pi} \int_0^{\sqrt{E_b}} \int_0^{\sqrt{E_b}} K(L_1, L_2)\, P(L_1, L_2) dL_1\, dL_2$$

where

$$(37) \qquad K(L_1, L_2) = \int_0^{\pi/2} \exp\left[- \frac{L_1^2\, L_2^2 / N_o}{L_1^2 \cos^2\theta + L_2^2 \sin^2\theta} \right] d\theta$$

and $P(L_1, L_2)$ is the joint probability density function for the variable L_1 and L_2. Similar expressions were derived for the conditional bit error probabilities P_0 and P_1. The expressions were numerically evaluated for the special case where the sixteen possible four-bit sequences are equally probable, i.e., each sequence occurs with a probability of one-sixteenth. Huff assumed 1) that the timing error process is independent of the noise processes n_{xm} and n_{ym}, 2) that the timing error is slowly varying with respect to the data bit rate, and 3) that the area under the tails of the Gaussian distribution function of the bit timing error for $|\epsilon| < T_b/2$ is small compared to the bit error probability, i.e., that L_1 and L_2 are essentially confined to the interval $(0, \sqrt{E_b})$.

Sample results showing P_{E_ϵ}, P_0, and P_1 as a function of E_b/N_o for $\bar{\epsilon}_n = 0$ and $\sigma_{\epsilon n} = 0.08$, where $\bar{\epsilon}_n = \bar{\epsilon}/T_b$ and $\sigma_{\epsilon n} \equiv \sigma_\epsilon / T_b$, are given

in Fig. 6. The theoretical results can also be presented in terms of a normalized ratio β/β_0, where β_0 and β are defined as the bit energy to noise density ratios required to maintain a given bit error probability under conditions of perfect and imperfect bit synchronization, respectively. Figure 7 shows the values of the ratio β/β_0 as a function of $\sigma_{\epsilon n}$ for several different bit timing offsets, and for $P_{E_\epsilon} = 10^{-5}$. Note that a small bit timing jitter ($\sigma_{\epsilon n} \sim 0.01$, $\bar{\epsilon}_n = 0$) causes performance to degrade less than 3% (in terms of β/β_0); in most cases such a loss would be considered insignificant. However, a moderate bit timing jitter ($\sigma_{\epsilon n} \approx 0.06$) causes performance to degrade more than 35% -- a relatively large loss.

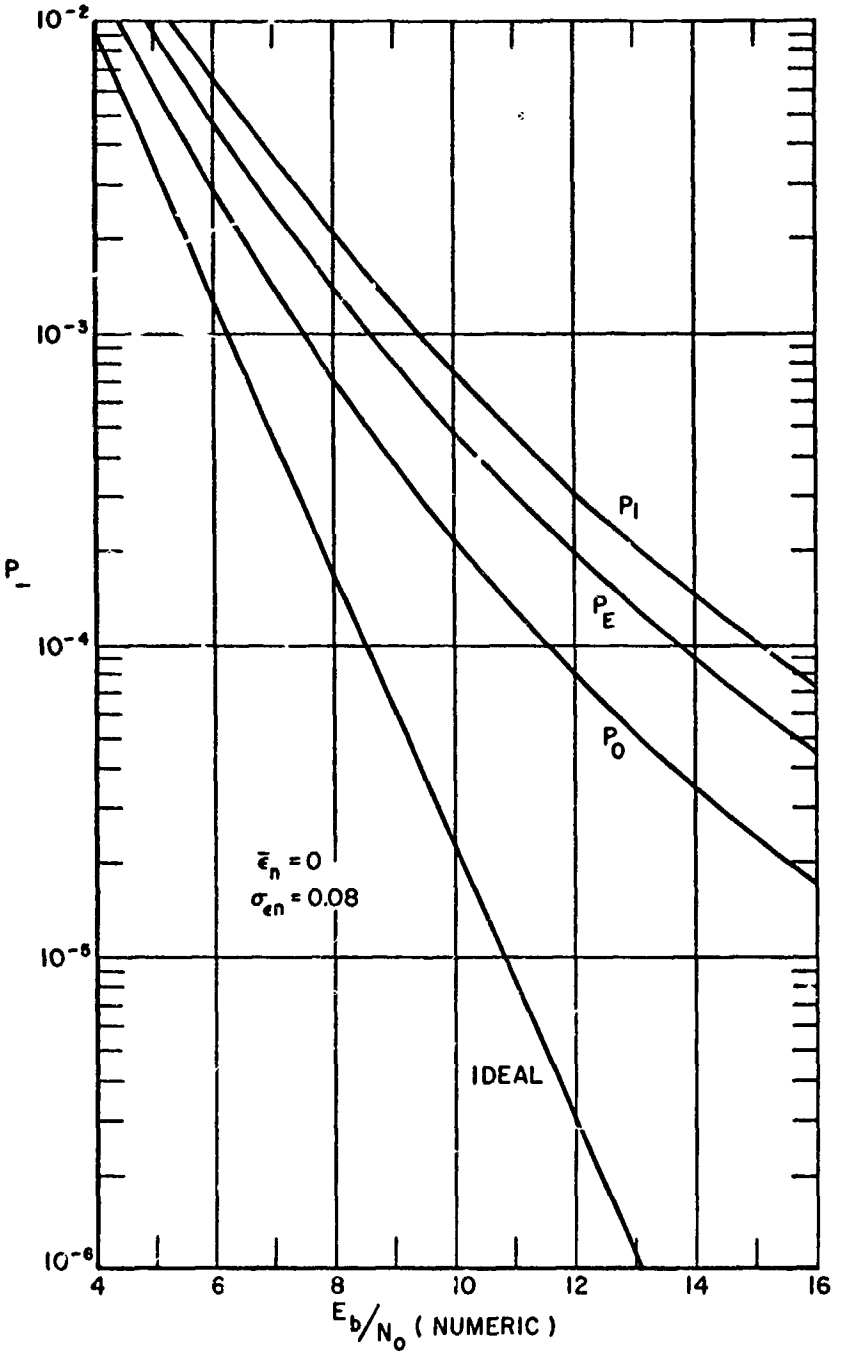

Fig. 6. The error probabilities P_E, P_0, and P_1 versus the bit energy to noise density ratio of the imperfectly-timed DD; $\bar{\epsilon}_n = 0$, $\sigma_{\epsilon n} = 0.08$.

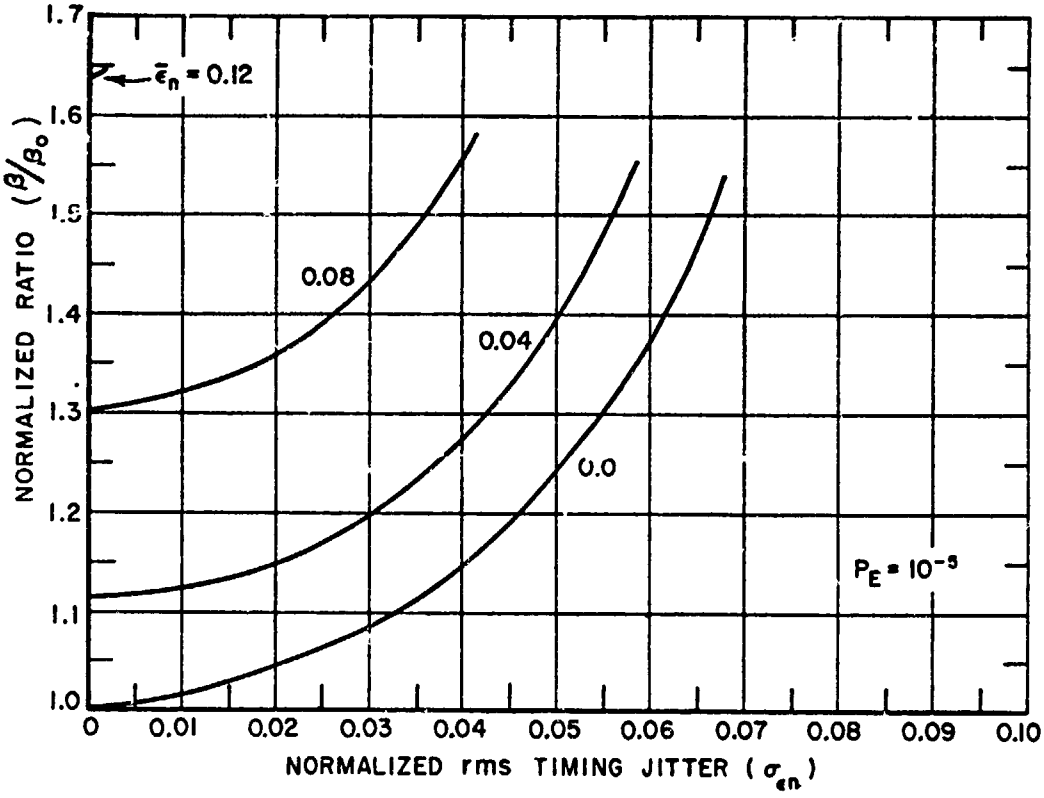

Fig. 7. The ratio β/β_0 versus the normalized timing jitter for selected values of the bit timing offset; $P_E = 10^{-5}$.

CHAPTER III
THE EFFECTS OF FREQUENCY UNCERTAINTY ON THE BIT ERROR PROBABILITY

A. Introduction

In this section, an expression for the bit error probability as a function of the frequency offset, Δf_o, and the bit energy to noise density ratio, with $\epsilon = 0$ and $\delta = 0$, will be derived. Much of the analysis parallels the approach used by Huff[1] in his analysis of the imperfectly-timed DD.

B. Preliminary Signal Analysis

When the phase angle $\alpha - \gamma$ [see Eqs. (10) and (11)] changes only a few degrees in adjacent bit intervals, the frequency offset does not change with time, and $\epsilon = \delta = 0$, Eqs. (10) and (11) become*

$$(38) \qquad S_{xi} = \frac{\sqrt{E_b}}{2\Delta\omega_o T_b} \left[\sin(\pi i_1 + \Delta\omega_o T_b + \beta) - \sin(\pi i_1 + \beta) + \sin(\pi i_1 - \beta) - \sin(\pi i_1 - \Delta\omega_o T_b - \beta)\right]$$

and

$$(39) \qquad S_{yi} = -\frac{\sqrt{E_b}}{2\Delta\omega_o T_b} \left[\cos(\pi i_1 + \beta) - \cos(\pi i_1 + \Delta\omega_o T_b + \beta) - \cos(\pi i_1 - \Delta\omega_o T_b - \beta) + \cos(\pi i_1 - \beta)\right]$$

*Again, m is set equal to 1 for convenience of notation.

where

$$\beta = \alpha - \gamma \quad . \tag{40}$$

Using these expressions in conjunction with Eq. (18) and employing the appropriate trigonometric identities, the expression for $\bar{S}_1$ reduces to

$$\bar{S}_1(\Delta\omega_o) = L_1 \left[\cos\left(\beta + \frac{\Delta\omega_o T_o}{2}\right)\hat{\phi}_x - \sin\left(\beta + \frac{\Delta\omega_o T_b}{2}\right)\hat{\phi}_y \right] \tag{41}$$

where

$$L_1 \equiv \sqrt{E_b}\, \frac{\sin(\Delta\omega_o T_b/2)}{\Delta\omega_o T_b/2} \quad . \tag{42}$$

The relation of $\bar{S}_1$ to the $\hat{\phi}_x, \hat{\phi}_y$ coordinate frame is shown in Fig. 8. The following relations are readily derived from Eq. (41):

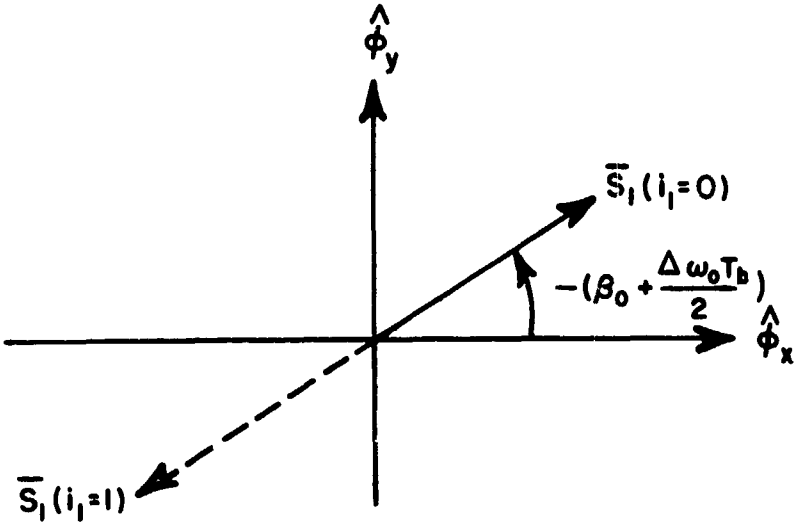

Fig. 8. The relationship of $\bar{S}_1$ to the $\hat{\phi}_x, \hat{\phi}_y$ coordinate frame with frequency offset.

(43) $$\lim_{\Delta\omega_o \to 0} \bar{S}_1(\Delta\omega_o) \equiv \bar{S}_1(0) = \sqrt{E_b}\ \cos \pi i_1 [\cos\beta \hat{\phi}_x - \sin\beta \hat{\phi}_y]$$

(44) $$|\bar{S}_1(\Delta\omega_o)| = L_1$$

and

(45) $$\angle \bar{S}_1(\Delta\omega_o) - \angle \bar{S}_1(0) = -\frac{\Delta\omega_o T_b}{2} \text{ radians (counterclockwise positive)} .$$

A new coordinate frame, (x', y'), in which $\bar{S}_1$ is aligned with the x' axis can be obtained by rotating the $(\hat{\phi}_x, \hat{\phi}_y)$ frame $(-\beta - \Delta\omega_o T_b/2 + \pi i_1)$ radians in the counterclockwise direction. In this new frame of reference, $\bar{S}_1$ can be expressed simply as

(46) $$\bar{S}_1 = L_1 \hat{a}_{x'} ,$$

where $\hat{a}_{x'}$ is a unit vector in the plus x' direction. By employing the same assumptions used to derive S_{x1} and S_{y1}, the components of $\bar{S}_2$ in the original reference frame are found to be given by

(47) $$S_{x2} = L_1 \cos \pi i_2 \cos(3\Delta\omega_o T_b/2 + \beta)$$

(48) $$S_{y2} = - L_1 \cos \pi i_2 \sin(3\Delta\omega_o T_b/2 + \beta)$$

and thus

(49) $$\bar{S}_2 = L_1 \cos \pi i_2 [\cos(3\Delta\omega_o T_b/2 + \beta)\hat{\phi}_x - \sin(3\Delta\omega_o T_b/2 + \beta)\hat{\phi}_y] .$$

In the (x', y') coordinate frame, $\bar{S}_2$ is expressible as

$$\bar{S}_2 = L_i \cos \pi \delta_i \, (\cos \Delta\omega_o T_b \, \hat{a}_{x'} - \sin \Delta\omega_o T_b \, \hat{a}_{y'}) \tag{50}$$

where

$$\delta_i = |i_2 - i_1| = \begin{cases} 1 & \text{if the data bit is a "1"} \\ 0 & \text{if the data bit is a "0"} \end{cases} . \tag{51}$$

Through inspection of Eqs. (46) and (50) it can be see that

$$|\bar{S}_2| = |\bar{S}_1| = L_1 \tag{52}$$

and

$$\angle \bar{S}_2 - \angle \bar{S}_1 = - \Delta\omega_o T_b \quad . \tag{53}$$

That is, the frequency offset causes the magnitude of the signal vectors to be reduced by the factor $\frac{\sin(\Delta\omega_o T_b/2)}{\Delta\omega_o T_b/2}$ and introduces a phase shift between $\bar{S}_2$ and $\bar{S}_1$. Neither the frequency offset nor the coordinate rotation affect the statistics of the noise components and thus $n_{x'1}$, $n_{x'2}$, $n_{y'1}$ and $n_{y'2}$ are samples from independent, zero-mean Gaussian processes having variance equal to $N_o/2$.

C. The Expression for the Bit Error Probability

In the (x', y') frame, the vectors $\bar{Z}_1$ and $\bar{Z}_2$ are expressible as

$$\bar{Z}_1 = e_{x'1} \, \hat{a}_{x'} + e_{y'1} \, \hat{a}_{y'} \tag{54}$$

and

$$\overline{Z}_2 = e_{x'2}\,\hat{a}_{x'} + e_{y'2}\,\hat{a}_{y'} \quad , \tag{55}$$

where

$$e_{x'1} = L_1 + n_{x'1} \tag{56}$$

$$e_{y'1} = n_{y'1} \tag{57}$$

$$e_{y'2} = -\,L_1 \cos \pi \delta_i \sin \Delta\omega_o T_b + n_{y'2} \tag{58}$$

and

$$e_{x'2} = L_1 \cos \pi \delta_i \cos \Delta\omega_o T_b + n_{x'2} \quad . \tag{59}$$

Sample values of $\overline{Z}_1$ and $\overline{Z}_2$ for the case $i_1 = i_2$ are shown in Fig. 9. The angle between the vectors $\overline{S}_1$ and $\overline{Z}_1$, measured in the counter-clockwise sense (see Fig. 9), is defined as ψ_1. Similarly, the angle between $\overline{S}_2$ and $\overline{Z}_2$ is defined as ψ_2. For this particular example, $\left|\psi_1 + \Delta\omega_o T_b - \psi_2\right| < \frac{\pi}{2}$; thus, $\overline{Z}_1 \cdot \overline{Z}_2 > 0$ and the receiver decides correctly that a zero was transmitted. Since the probability density functions of ψ_1 and ψ_2 are even, frequency offset introduces an asymmetrical dependence of the bit error probability on the noise which degrades performance.

Assuming that the threshold voltage, V_T, is zero, the error probabilities P_0 and P_1 are given by

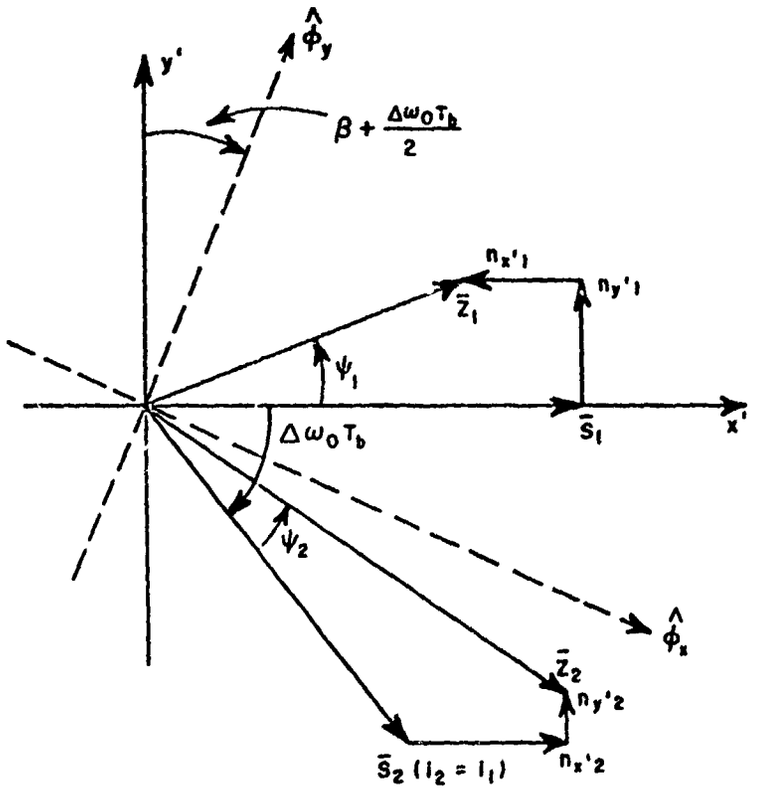

Fig. 9. Relationship of the signal vectors $\bar{Z}_1$ and $\bar{Z}_2$ to the $\hat{\phi}_x$, $\hat{\phi}_y$ and the x', y' coordinate reference frames.

(60) $$P_0 = P_{rob.}\ (\bar{Z}_i \cdot \bar{Z}_2 < 0 / \delta_i = 0)$$

(61) $$P_1 = P_{rob.}\ (\bar{Z}_1 \cdot \bar{Z}_2 > 0 / \delta_i = 1)$$

An expression for P_0 will now be derived.

Since $n_{x'1}$ and $n_{y'1}$ are statistically independent samples from zero mean Gaussian processes, each with variance $N_0/2$, the conditional joint density function for $e_{x'1}$ and $e_{y'1}$ can be written as [see Eqs. (56) and (57)]

$$(62)\qquad p(e_{x'_1}, e_{y'_1} \mid \sqrt{E_b}, \Delta\omega_o) = p(e_{x'_1}, e_{y'_1} \mid L_1) = \frac{1}{\pi N_o} \exp\left[- \frac{(e_{x'_1} - L_1)^2 + e_{y'_1}^2}{N_o} \right] \quad .$$

The signal components $e_{x'_1}$ and $e_{y'_1}$ can be written in terms of $\bar{Z}_1$ and ψ_1 as

$$\left.\begin{aligned} (63)\qquad e_{x'_1} &= |\bar{Z}_1| \cos\psi_1 \\ (64)\qquad e_{y'_1} &= |\bar{Z}_1| \sin\psi_1 \end{aligned}\right\} \quad -\pi < \psi_1 < \pi \quad .$$

The conditional probability density function of ψ_1, given L_1, is found by substituting Eqs. (63) and (64) into Eq. (62) and then employing a well-known transformation technique[8] to obtain

$$(65)\qquad P(\psi_1 \mid L_1) = \frac{1}{2\pi} \exp\left[- \frac{L_1^2}{N_o} \right] + \frac{1}{\sqrt{2\pi}} \exp\left[- \frac{L_1^2 \sin^2\psi_1}{N_o} \right] \cdot L_1 \sqrt{\frac{2}{N_o}} \cos\psi_1 \left[\frac{1}{2} + Q(L_1, \psi_1) \right]$$

where

$$(66)\qquad Q(L, \psi) = \frac{1}{\sqrt{2\pi}} \int_0^{L\sqrt{\frac{2}{N_o}} \cos\psi_1} \exp\left[- \frac{u^2}{2} \right] du \quad .$$

Next, assuming ψ_1 given, a new $(\bar{x}, \bar{y})$ coordinate frame is formed by rotating the (x', y') frame in the counter-clockwise direction so that the signal vector $\bar{Z}_1$ is aligned with the positive $\bar{x}$ axis. Thus, in terms of the $(\bar{x}, \bar{y})$ frame,

(67) $$e_{\overline{x}2} = (L_1 \cos\Delta\omega_o T_b \cos\psi_1 + L_1 \sin\Delta\omega_o T_b \sin\psi_1) \cos\pi\delta_i + n_{\overline{x}2}$$

(68) $$e_{\overline{y}2} = [-L_1 \sin\Delta\omega_o T_b \cos\psi_1 + L_1 \cos\Delta\omega_o T_b \sin\psi_1] \cos\pi\delta_i + n_{\overline{y}2}$$

which, for $\delta_i = 0$, reduces to

(69) $$e_{\overline{x}2} = L_1 \cos(\Delta\omega_o T_b - \psi_1) + n_{\overline{x}2}$$

(70) $$e_{\overline{y}2} = L_1 \sin(\Delta\omega_o T_b - \psi_1) + n_{\overline{y}2}$$

where

(71) $$n_{\overline{x}2} = n_{x'2} \cos\psi_1 + n_{y'2} \sin\psi_1$$

(72) $$n_{\overline{y}2} = n_{y'2} \cos\psi_1 - n_{x'2} \sin\psi_1 \quad .$$

As before, the $n_{\overline{x},\overline{y}i}$ are samples from statistically independent, zero-mean Gaussian processes, each with variance $N_o/2$.

Examination of the vector components of $\overline{Z}_2$ and $\overline{Z}_1$ in the $(\overline{x},\overline{y})$ frame reveals that $e_{\overline{x}2}$ is proportional to the dot product $\overline{Z}_1 \cdot \overline{Z}_2$. Thus, $e_{\overline{x}2} = 0$ corresponds to the decision boundary $|\psi_2 - \Delta\omega_o T_b - \psi_1| = \frac{\pi}{2}$. Therefore, Eqs. (60) and (61) reduce to

(73) $$P_0 = P_{rob}\,(e_{\overline{x}2} < 0 \,|\, L_1, \delta_i = 0)$$

(74) $$P_1 = P_{rob}\,(e_{\overline{x}2} \geq 0 \,|\, L_1, \delta_i = 1) \quad .$$

From Eq. (67), the conditional density function for $e_{\overline{x}2}$ can be written as

$$(75) \qquad p(e_{\overline{x}2}|\Delta\omega_o, \delta_i = 0) = \frac{1}{\sqrt{\pi N_o}} \exp\left[-\frac{1}{N_o}[e_{\overline{x}2} - L_1 \cos(\Delta\omega_o T_b - \psi_1)]^2\right]$$

By the chain rule for marginal and joint density functions[12],

$$(76) \qquad p(e_{\overline{x}2}, L_1, \psi_1|\Delta\omega_o, \delta_i=0) = p(e_{\overline{x}2}|L_1, \Delta\omega_o, \psi_1, \delta_i=0) \cdot p(\psi_1|L_1, \Delta\omega_o, \delta_i=0)\, p(L_1|\Delta\omega_o, \delta_i=0) \quad .$$

Integrating both sides of Eq. (76) over the range of ψ_1 and L_1, it is found that

$$(77) \qquad p(e_{\overline{x}2}|\Delta\omega_o, \delta_i=0) = \int_{L_1}\int_{\psi_1} p(e_{\overline{x}2}|L_1, \Delta\omega_o, \psi_1, \delta_i=0) \cdot p(\psi_1|L_1, \Delta\omega_o, \delta_i=0)\, p(L_1|\Delta\omega_o, \delta_i=0)\, d\psi_1\, dL_1 \quad .$$

For a given $\Delta\omega_o$ and for $\delta_i = 0$, L_1 is a constant. Thus

$$(78) \qquad p(L_1|\Delta\omega_o, \delta_i=0) = \delta\left[L_1 - \sqrt{E_b}\left(\frac{\sin(\Delta\omega_o T_b/2)}{\Delta\omega_o T_b/2}\right)\right]$$

where $\delta(x)$ is the Dirac-delta function. Moreover, the value of ψ_1 is independent of the frequency offset and the phase of the succeeding bit interval. Therefore,

$$(79) \qquad p(\psi_1|L_1, \Delta\omega_o, \delta_i = 0) = p(\psi_1|L_1) \quad .$$

Utilizing the relations in Eqs. (78) and (79), Eq. (77) reduces to

$$(80) \qquad p(e_{\overline{x}2} \mid L_1, \Delta\omega_o, \delta_i=0) = \int_{\psi_1} p(e_{\overline{x}2} \mid L_1, \Delta\omega_o, \psi_1, \delta_i=0)\, p(\psi_1 \mid L_1) d\psi_1 \ .$$

Substituting Eq. (80) into Eq. (73), the probability of error given that a "0" was transmitted becomes

$$(81) \qquad P_0 = \int_{-\infty}^{0} p(e_{\overline{x}2} \mid L_1, \Delta\omega_o, \delta_i=0)\, d\, e_{\overline{x}2}$$

$$= \int_{-\pi}^{\pi} \int_{-\infty}^{0} \frac{1}{\sqrt{\pi N_o}} \exp\left[-\frac{1}{N_o}[e_{\overline{x}2} - L_1 \cos(\Delta\omega_o T_b - \psi_1)]^2\right] de_{\overline{x}2} \cdot p(\psi_1 \mid L_1) d\psi_1$$

$$= \int_{-\pi}^{\pi} \left[\frac{1}{2} - Q(L_1, \Delta\omega_o T_b - \psi_1)\right] p(\psi_1 \mid L_1) d\psi_1 \ .$$

Simularly, P_1 is found to be given by

$$(82) \qquad P_1 = \int_0^{\infty} p(e_{\overline{x}2} \mid L_1, \Delta\omega_o, \delta_i=1)\, de_{\overline{x}2}$$

$$= \int_{-\pi}^{\pi} \int_0^{\infty} \frac{1}{\sqrt{\pi N_o}} \exp\left[-\frac{1}{N_o}[e_{\overline{x}2} + L_1 \cos(\Delta\omega_o T_b - \psi_1)]^2\right] de_{\overline{x}2} \cdot p(\psi_1 \mid L_1) d\psi_1 \ .$$

By an appropriate change of variables, P_0 and P_1 can be shown to be equal; thus the bit error probability is independent of the transmitted symbol. In the remainder of the analysis, it will be assumed that $\delta_i = 0$.

Now, on substituting Eq. (65) into Eq. (81), the expression for the total bit error probability can be written as

$$(83)\qquad P_E = P_0 = \frac{1}{4\pi}\int_{-\pi}^{\pi} \exp\left[-\frac{L_1^2}{N_o}\right] d\psi_1 + \frac{L_1}{4\sqrt{\pi N_o}}\int_{-\pi}^{\pi} \exp\left[-\frac{L_1^2 \sin^2\psi_1}{N_o}\right] \cdot \cos\psi_1\, d\psi_1$$

$$- \frac{1}{2\pi}\int_{-\pi}^{\pi} Q(L_1, \Delta\omega_o T_b - \psi_1) \exp\left[-\frac{L_1^2}{N_o}\right] d\psi_1$$

$$- \frac{L_1}{2\sqrt{\pi N_o}}\int_{-\pi}^{\pi} Q(L_1, \Delta\omega_o T_b - \psi_1) \exp\left[-\frac{L_1^2 \sin^2\psi_1}{N_o}\right] \cos\psi_1\, d\psi_1$$

$$+ \frac{L_1}{2\sqrt{\pi N_o}}\int_{-\pi}^{\pi} Q(L_1, \psi_1) \exp\left[-\frac{L_1^2 \sin^2\psi_1}{N_o}\right] \cos\psi_1\, d\psi_1$$

$$- \frac{L_1}{\sqrt{\pi N_o}}\int_{-\pi}^{\pi} Q(L_1, \psi_1) Q(L_1, \Delta\omega_o T_b - \psi_1) \exp\left[-\frac{L_1^2 \sin^2\psi_1}{N_o}\right] \cdot \cos\psi_1\, d\psi_1 \,.$$

Fortunately, this equation can be simplified by utilizing symmetry properties of the integrands. It can be shown that

$$(84)\qquad \int_{-\pi}^{\pi} Q(L_1, \Delta\omega_o T_b - \psi_1) \exp\left[-\frac{L_1^2}{N_o}\right] d\psi_1 = 0$$

$$(85)\qquad \int_{-\pi}^{\pi} Q(L_1, \Delta\omega_o T_b - \psi_1) Q(L_1, \psi_1) \exp\left[-\frac{L_1^2 \sin^2\psi_1}{N_o}\right] \cos\psi_1\, d\psi_1 = 0$$

$$(86)\qquad \int_{-\pi}^{\pi} \exp\left[-\frac{L_1^2 \sin^2\psi_1}{N_o}\right] \cos\psi_1\, d\psi_1 = 0$$

and

$$(87)\qquad \int_{-\pi}^{\pi} Q(L_1,\psi_1)\exp\left[-\frac{L_1^2\sin^2\psi_1}{N_o}\right]\cos\psi_1\,d\psi_1$$

$$= 4\int_{0}^{\pi/2} Q(L_1,\psi_1)\exp\left[-\frac{L_1^2\sin^2\psi_1}{N_o}\right]\cos\psi_1\,d\psi_1 \ .$$

The expression for P_E in Eq. (83) is now expressible in the form

$$(88)\qquad P_E = \frac{1}{2}\ \exp\left[-\frac{L_1^2}{N_o}\right] + E_1 - E_2$$

where

$$(89)\qquad E_1 = \frac{2L_1}{\sqrt{\pi N_o}}\int_0^{\pi/2} Q(L_1,\psi_1)\ \exp\left[-\frac{L_1^2\sin^2\psi_1}{N_o}\right]\ \cos\psi_1\,d\psi_1$$

and

$$(90)\qquad E_2 = \frac{L_1}{2\sqrt{\pi N_o}}\int_{-\pi}^{\pi} Q(L_1,\Delta\omega_o T_b-\psi_1)\exp\left[-\frac{L_1^2\sin^2\psi_1}{N_o}\right]\cos\psi_1\,d\psi_1 \ .$$

It is easy to show that[1]

$$(91)\qquad E_1 = \frac{1}{2} - \frac{1}{2}\ \exp\left[-\frac{L_1^2}{N_o}\right] \ .$$

The expression for E_2 is evaluated in Appendix B to give

$$(92)\qquad E_2 = \frac{1}{2} - \frac{1}{\pi}\int_0^{\pi/2}\exp\left[-\frac{L_1^2\,L_2^2/N_o}{L_1^2\cos^2\theta + L_2^2\sin^2\theta}\right]\ d\theta$$

$$+\ \frac{L_1}{\pi\sqrt{2N_o}}\int_{-\pi/2}^{\pi/2}\int_{L_1\sqrt{\frac{2}{N_o}}\cos x\,\cos\Delta\omega_o T_b}^{L_1\sqrt{\frac{2}{N_o}}\cos(x+\Delta\omega_o T_b)}\exp\left[-\frac{u^2}{2}\right]\,du$$

$$\cdot\ \exp\left[-\frac{L_1^2\sin^2 x}{N_o}\right]\cos x\ dx$$

where

$$L_2 \equiv L_1 \cos \Delta\omega_o T_b \quad . \tag{93}$$

The desired expression for the bit error probability as a function of the frequency offset Δf_o and the bit energy to noise density ratio E_b/N_o is obtained by combining Eqs. (88), (91) and (92). In a form convenient for numerical computation, the result is

$$P_E(L_1, E_b/N_o, \Delta\omega_o) = \frac{1}{\pi} \int_0^{\pi/2} \exp\left[- \frac{L_1^2 L_2^2/N_o}{L_1^2 \cos^2\theta \quad L_2^2 \sin^2\theta} \right] d\theta \tag{94}$$

$$+ \frac{L_1}{\pi\sqrt{2N_o}} \int_{-\pi/2}^{\pi/2} \left\{ \int_{L_1\sqrt{\frac{2}{N_o}}\cos(x+\Delta\omega_o T_b)}^{L_1\sqrt{\frac{2}{N_o}}\cos x \cos\Delta\omega_o T_b} \exp\left(-\frac{u^2}{2}\right) du \right\}$$

$$\cdot \exp\left[- \frac{L_1^2 \sin^2 x}{N_o} \right] \cos x \, dx \quad .$$

The value of the first integral in the above expression depends on the projection of $\bar{S}_{m-1}$ onto $\bar{S}_m$ and has the same form as the function $K(L_1, L_2)$ defined by Huff [1] (see Eq. (37)). The second integral takes into account the asymmetrical dependence of the bit error probability on the noise introduced by frequency offset. Note that the result is invariant to the sign of the frequency offset and that, in the limit as $\Delta\omega_o$ goes to zero, Eq. (94) becomes the expression for the bit error probability of the ideal differential detector, given by Eq. (23).

D. Numerical Results

The expression for the bit error probability was evaluated numerically; the results are given in Fig. 10 for various normalized frequency offsets, $\Delta f_n = \Delta f_o T_b$, as a function of the bit energy to noise density ratio. These results can be presented in a different manner by plotting the additional signal power required to maintain a given bit error probability as a function of frequency offset. Calculated values of $\frac{\mu}{\mu_o}$ for selected bit error probabilities are shown in Fig. 11, where μ_o and μ have been defined as the bit energy to noise density ratios required to maintain the given bit error probability for zero and non-zero frequency offsets, respectively. The results indicate that a small frequency offset does not significantly degrade performance, but that efficiency drops sharply for larger offsets. For example, an offset of $(0.01)T_b$ results in an effective energy loss of less than 0.1 dB and could be tolerated in most applications. An offset of only $(0.05)T_b$, however, introduces a loss greater than 1 dB, which may be unacceptable.

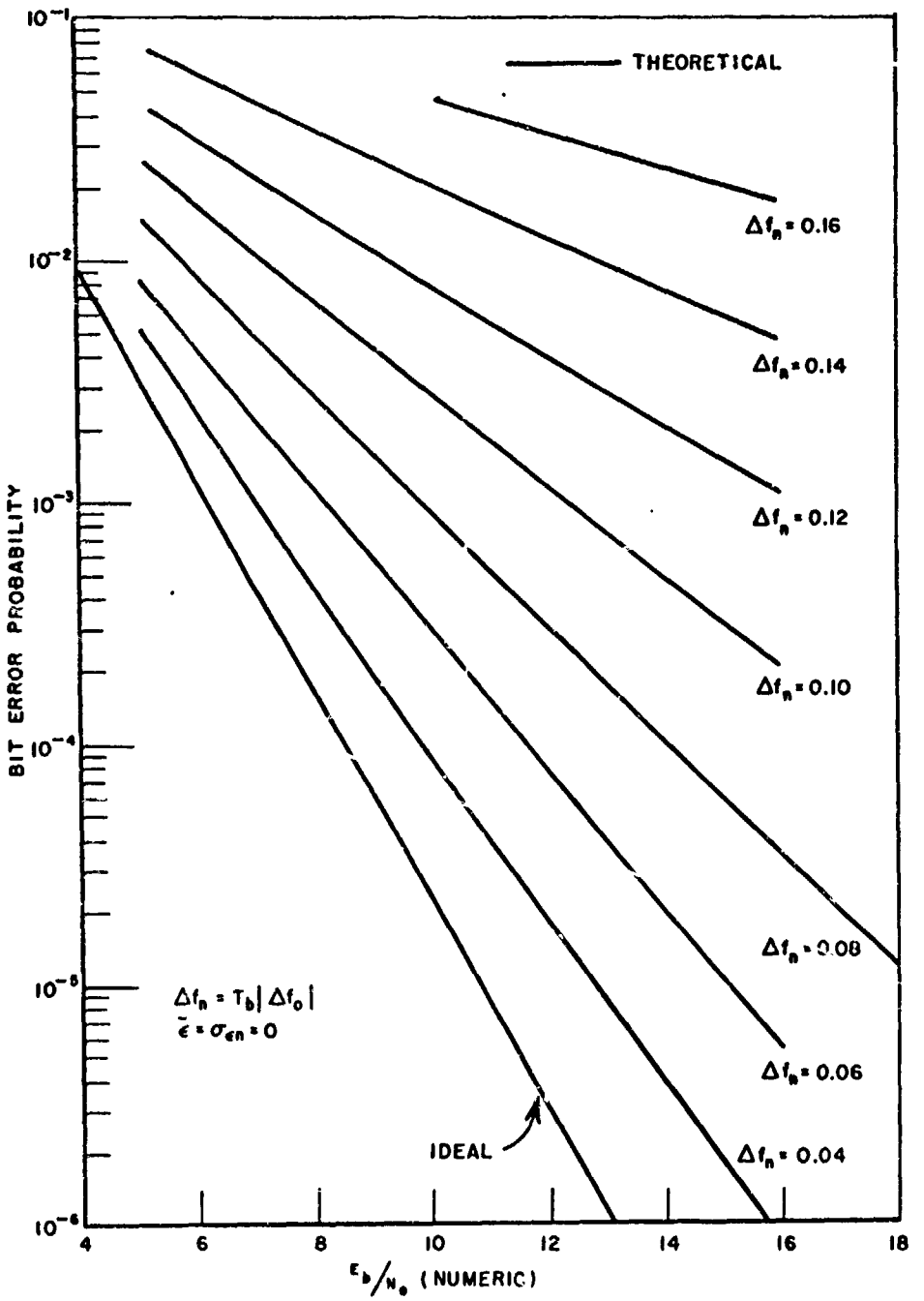

Fig. 10. The bit error probability versus the bit energy to noise density ratio for selected values of frequency offset.

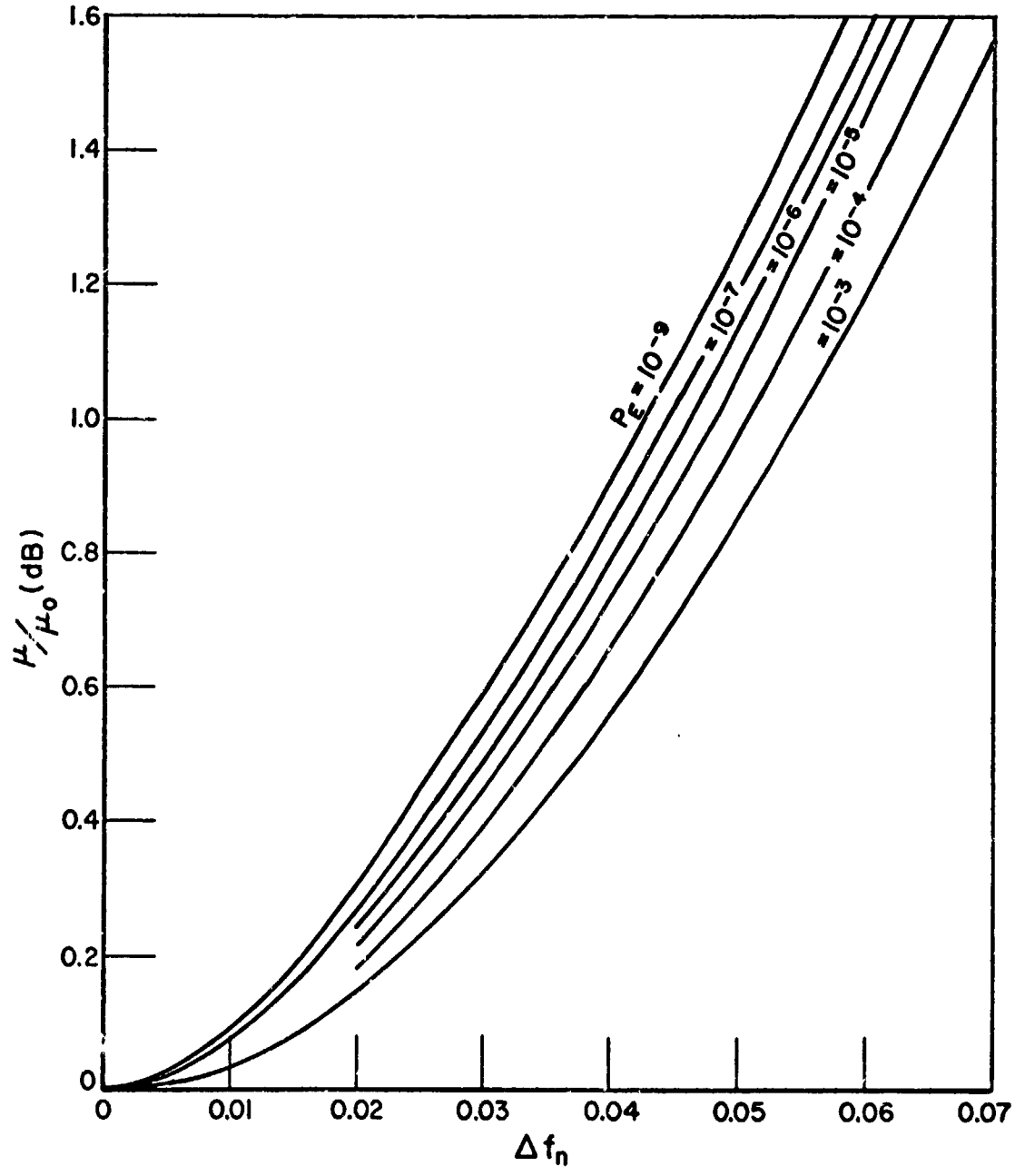

Fig. 11. The ratio μ/μ_o (see p. 38) versus frequency offset for selected values of the bit error probability.

CHAPTER IV
THE EXPERIMENTAL DIFFERENTIAL DETECTOR AND ASSOCIATED TEST CIRCUITS

A. Introduction

An experimental receiver was instrumented to test the validity of the analytical results and to provide additional results for cases which are extremely difficult to investigate analytically. In what follows, the experimental DD and the associated test circuitry are described in some detail.

B. Description of the Differential Detector

A block diagram of the experimental DD is shown in Fig. 12. The input signal Z(t) represents the received waveform at a 30 MHz IF. This signal is first split into two components having equal magnitudes and phase using a hybrid divider. Two switch type balanced mixers, driven by quadrature local oscillator signals, are used to down-convert these components to generate two (approximately) orthogonal baseband signals, $\xi_x(t)$ and $\xi_y(t)$. Each mixer is followed by a low-pass gain stage which has a bandwidth equal to about 1 MHz. In turn, the output of each gain stage is applied to an integrate/dump circuit. The dump time of each integrator is continuously variable from 350 nsec to

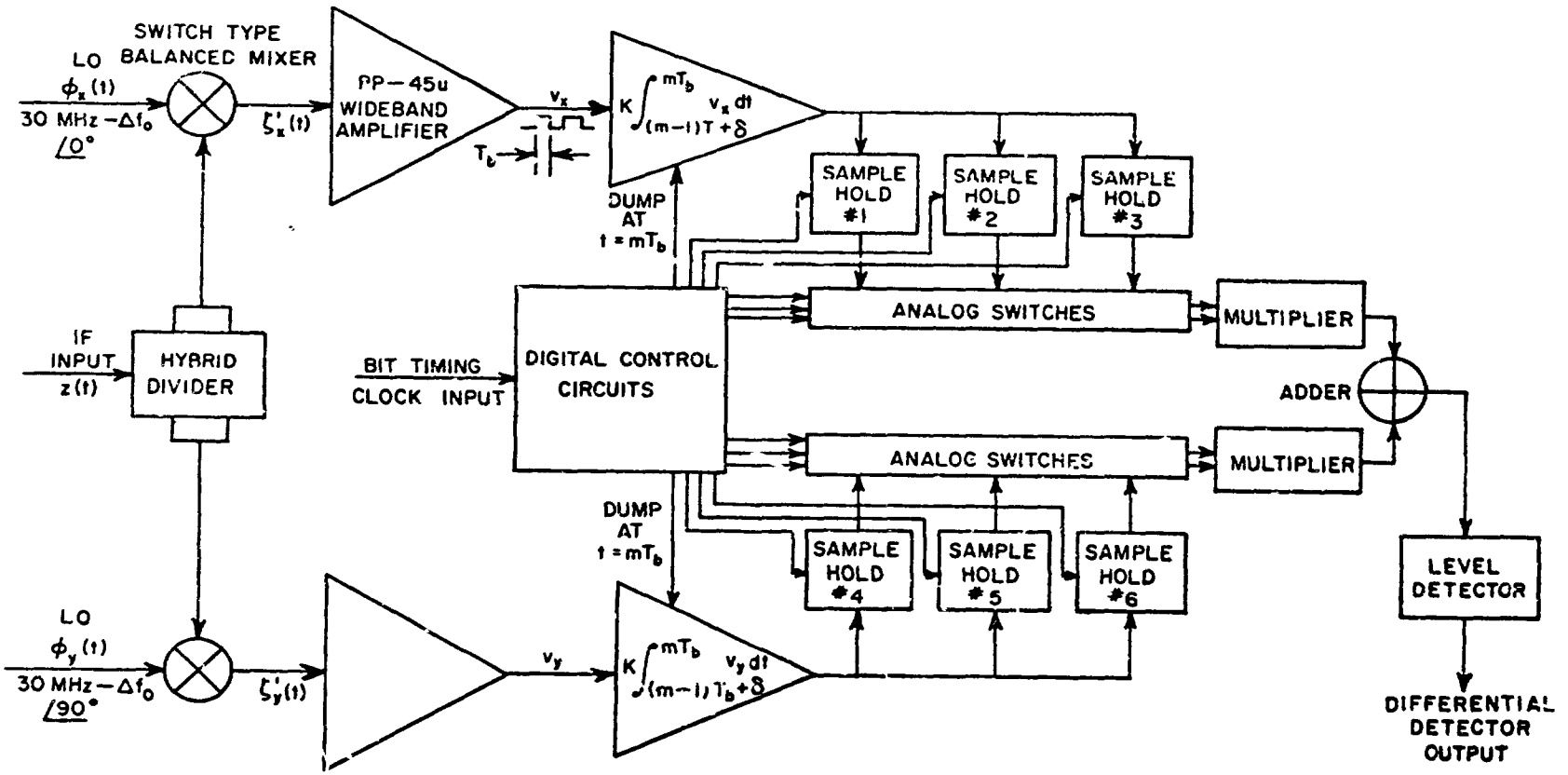

Fig. 12. A block diagram of the differential detector.

5 μsec. However, all results to be presented were obtained with δ set equal to 350 nsec. A detailed schematic diagram of the integrator circuitry is given in Appendix C.

The detector contains six separately controlled sample/hold (S/H) modules, three in each orthogonal channel. Each S/H module samples the appropriate integrator's output at the end of every third interval and holds it for two integration intervals, i.e., for $2T_b$ seconds. Thus, each S/H circuit tracks for T_b seconds and holds for $2T_b$ seconds. The three S/H modules in each channel allows each integrator output to be sampled at the end of every bit interval by appropriately staggering the hold commands. At a given instant of time t satisfying $mT_b < t < (m+1)T_b$, stored samples of the integrator outputs for the (m-1)-th and the (m)-th bit intervals (e.g., e_{xm}, $e_{x(m-1)}$, e_{ym}, and $e_{y(m-1)}$) are available at four of the six S/H outputs, so that the dot product $\overline{Z}_m \cdot \overline{Z}_{(m-1)} = e_{xm}e_{x(m-1)} + e_{ym}e_{y(m-1)}$ can be formed in the multiplier circuit. Eight analog switching circuits are used to control the order in which the S/H outputs are multiplied, as shown in Table 2 for the $\hat{\phi}_x$ component; the arrangement is the same for the $\hat{\phi}_y$ component.

The products $e_{xm}e_{x(m-1)}$ and $e_{ym}e_{y(m-1)}$ are formed by two four-quadrant multipliers. At the multiplier outputs, the message carrying component of the signal is a binary waveform modulated by a sinusoid having a frequency equal to $2\Delta f_o$. Ideally, the sinusoidal

TABLE 2
The cyclic arrangement of the analog switching and sample-hold functions

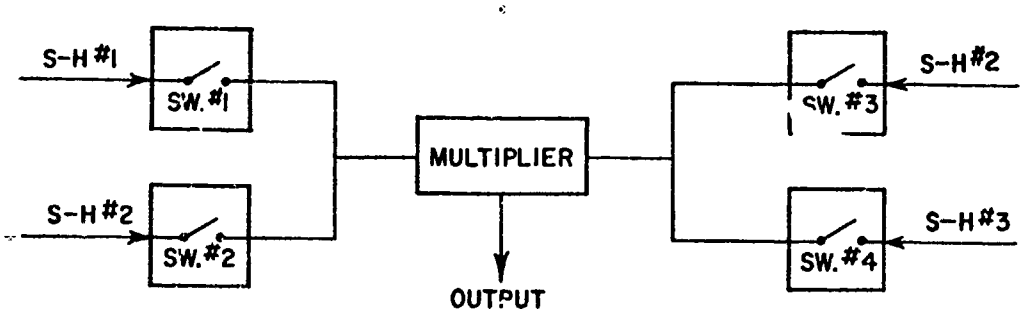

Signalling Interval	Sample-Hold Inputs #1	#2	#3	Analog Switches #1	#2	#3	#4	Sample-Hold Inputs Multiplied (Multiplier Output)
m	HOLD	HOLD	SAMPLE	ON	OFF	ON	OFF	#1 x #2
m+1	SAMPLE	HOLD	HOLD	OFF	ON	OFF	ON	#2 x #3
m+2	HOLD	SAMPLE	HOLD	ON	OFF	OFF	ON	#1 x #3
m+3	HOLD	HOLD	SAMPLE	ON	OFF	ON	OFF	#1 x #2
m+4	SAMPLE	HOLD	HOLD	OFF	ON	OFF	ON	#2 x #3
m+5	HOLD	SAMPLE	HOLD	ON	OFF	OFF	ON	#1 x #3
.	.	.	.	.	.	.	.	.
.	.	.	.	.	.	.	.	
.	.	.	.	.	.	.	.	. . .

modulation on the output of one multiplier is 180° out of phase with respect to the modulation on the second multiplier's output. The two multiplier outputs are added using an (inverting) operational amplifier to generate $\overline{Z}_m \cdot \overline{Z}_{(m-1)}$. Ideally, the sinusoidal modulation (at the frequency $2\Delta f_o$) at the amplifier inputs does not appear at the output. The signal representing $\overline{Z}_m \cdot \overline{Z}_{(m-1)}$ is then applied to a level detector to generate the detected bit stream. If the input to the level detector is greater than zero, the output of the level detector is a positive voltage; otherwise, the output is zero.

The experimental receiver was designed to give satisfactory performance for data bit rates up to 500 Kbps. However, at high bit rates, demodulator performance is degraded by bandlimiting, slew rate limiting, integrator dump time limitations, and other extraneous receiver imperfections (see Appendix C). At low bit rates, the time required to obtain an accurate measurement of the bit error probability is large. For these reasons, the experimental data to be presented was obtained with the rate set at an intermediate value, 50 Kbps. A list of receiver parameters for f_b = 50 Kbps is given in Appendix D.

C. Description of Peripheral Test Circuits

A block diagram of the circuits used to bench test the experimental differential detector is shown in Figs. 13a and 13b. These circuits were designed to perform the following functions;

(1) generation of the additive channel noise process, the bit timing error process, the data bit stream, and the transmitted waveform, (2) measurement of the bit timing error, the frequency offset, the signal to noise ratio, the BEP and the probability of two consecutive errors, and (3) computation of σ_ϵ^2 and $\bar{\epsilon}$. The basic operation of the peripheral circuitry is described in this section.

The bit timing jitter and the channel noise processes were derived from separate noise sources to ensure their statistical independence. Each source produced zero mean Gaussian noise in a band 7 MHz wide centered at 30 MHz. The spectra of the two noise voltages was flat to within ± 0.5 dB over the frequency range 30 MHz $\pm$ 1 MHz. A hybrid combiner was used to add the channel noise, n(t), to the

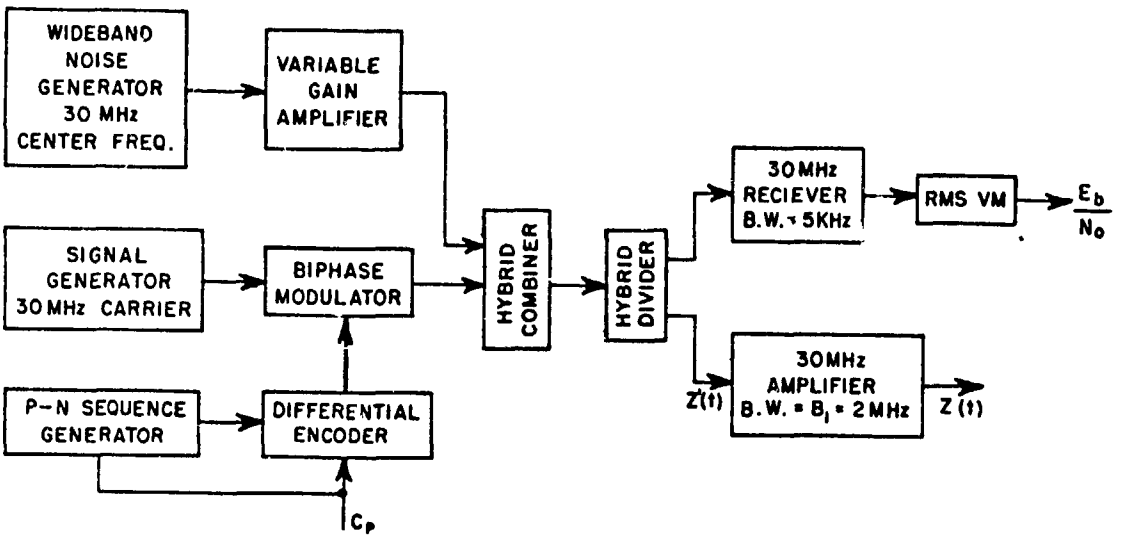

Fig. 13a. A block diagram of the peripheral test circuits used to generate the transmitted waveform.

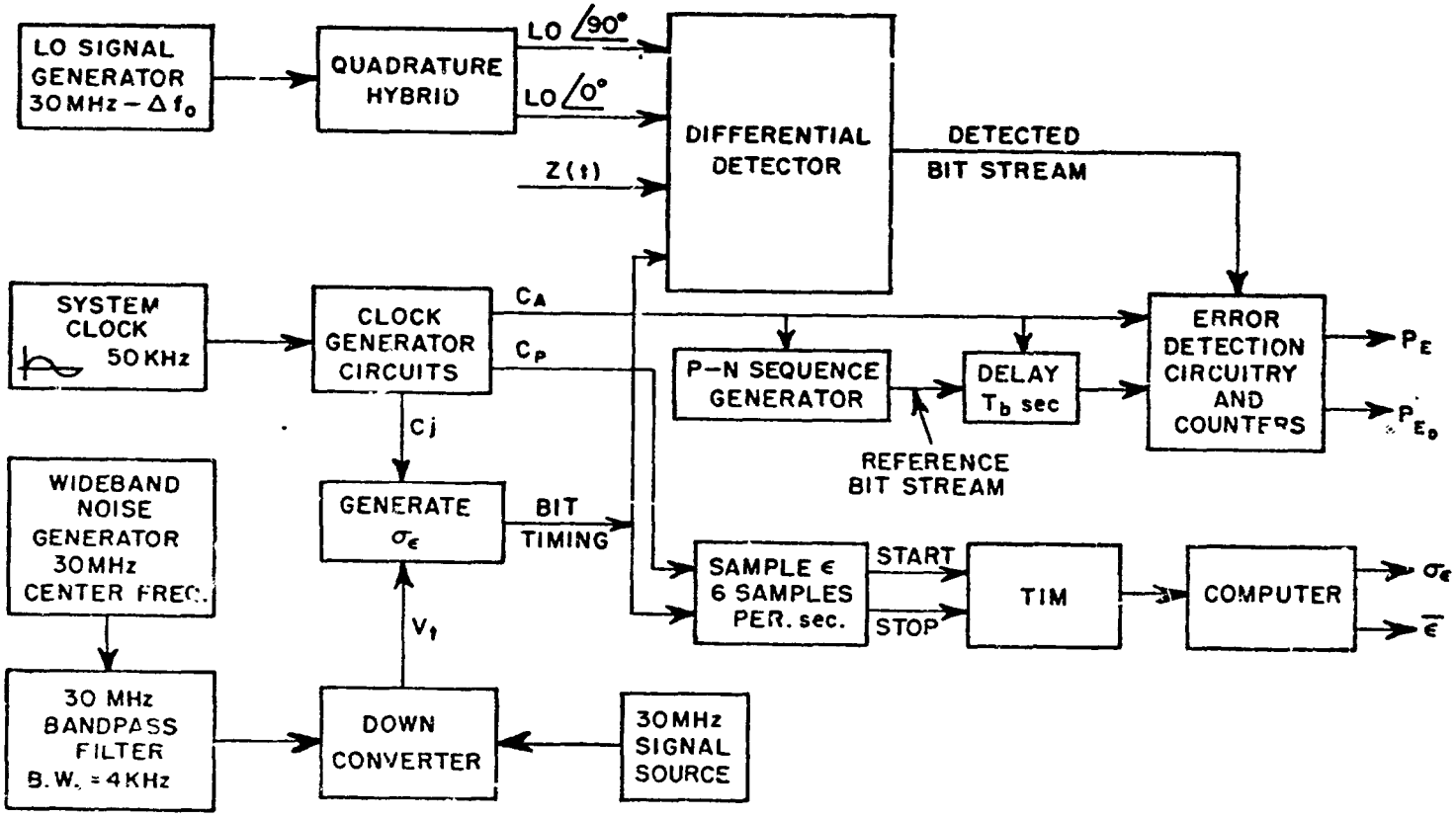

Fig. 13b. A block diagram of the peripheral test circuits used to generate receiver imperfections and to measure receiver performance.

transmitted waveform to obtain the signal $Z'(t)$. Since 2 MHz >> 50 Kbps, the noise voltage approximated a white Gaussian process. Due to a limitation in the dynamic range of the mixer stage at the DD input, the signal $Z'(t)$ was bandlimited to 2 MHz($=B_1$); the filter output was the receiver input $Z(t)$. The baseband noise used to generate bit timing error was obtained by down-converting the appropriate 30 MHz noise signal and filtering the resulting waveform to the desired bandwidth.

The data bit stream consisted of a maximum length 127-bit P-N sequence. The data bit stream was differentially encoded using the circuit diagrammed in Fig. 14 and then used to biphase modulate the 30 MHz carrier. In the theoretical analysis of the effects of bit timing error, each four bit sequence was assumed to occur in the encoded bit stream with equal likelihood. Using the 127-bit P-N sequence resulted in an approximation to this assumption, as illustrated by Table 3. The probability of occurrence of the {0, 0, 0, 0} sequence is equal to about 0.551, while the probability of occurrence of any other four bit sequence equaled about 0.063. Since bit timing error does not affect performance when {0, 0, 0, 0} is transmitted, the measured bit error probability should be slightly larger than the value determined theoretically. The effect is very small, however, since one less {0, 0, 0, 0} sequence per 127 sequences amounts to less than one percent.

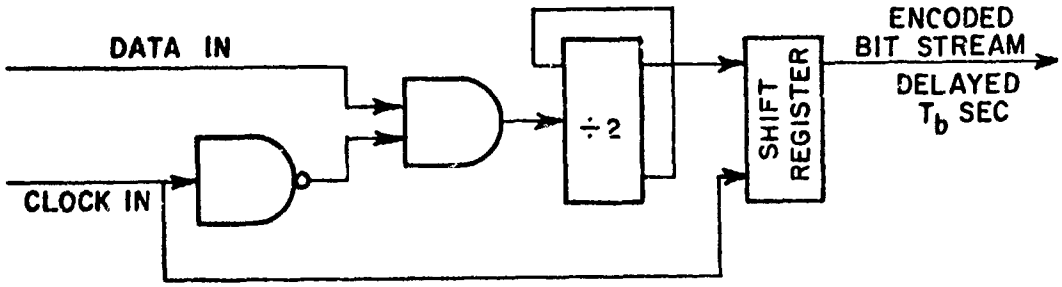

Fig. 14. A block diagram of the differential encoder.

TABLE 3
The probability of occurrence of each four bit sequence

Sequence	Probability of Occurrence
0000	0.0551
0001	0.0630
1000	"
1111	"
1110	"
0111	"
0110	"
0010	"
0011	"
1010	"
1011	"
1101	"
1100	"
0101	"
0100	"

The system clock, a 50 KHz sinusoid, is used to generate the absolute system clock, C_A, the phase adjustable clock, C_p, and the phase adjustable timing jitter clock, C_j. The absolute system clock, a square wave derived from the zero crossings of the 50 KHz system clock, is used to generate an error-free data bit stream for comparison with the receiver output. The phase adjustable system clock is used to generate the transmitted bit stream; the phase of C_p is adjusted to compensate for circuit delays with respect to C_A. The second adjustable system clock, C_j, is used to time the digital control circuits in the DD; its phase directly determines the bit timing offset $\bar{\epsilon}_n$.

The bit timing error is generated by comparing a baseband noise voltage with a sawtooth waveform. The period of the sawtooth equals the data bit length, T_b, as shown in Fig. 15, and its phase is determined by C_j. The noise voltage, V_t, is a narrowband, zero-mean Gaussian process with a bandwidth equal to 2 KHz. The sawtooth and noise voltages are compared using an analog comparator. The output of the comparator is a series of pulses whose leading edge remains in phase with the sawtooth and whose trailing edge is delayed t' seconds with respect to the leading edge (see Fig. 15):

$$t' = \frac{V_t}{2V_A} T_b + t_o \quad . \tag{95}$$

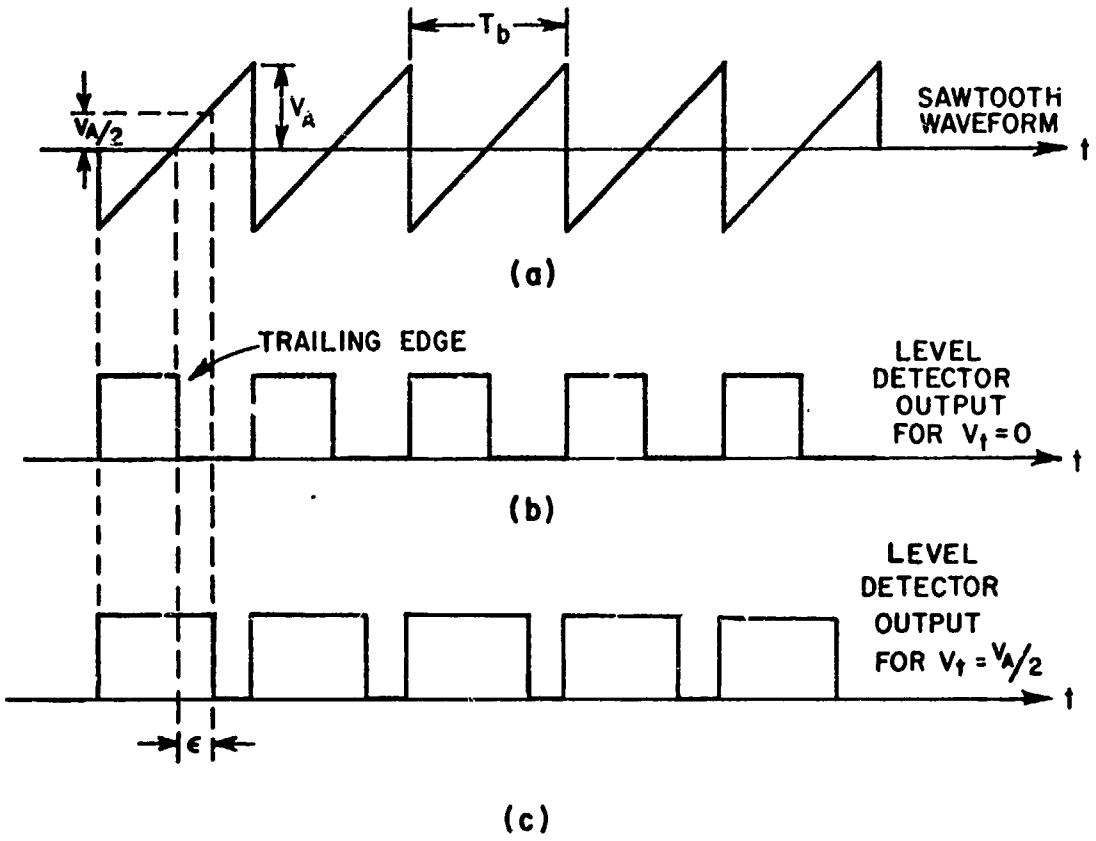

Fig. 15. Generation of bit timing jitter.

If V_t is assumed constant during each period of the sawtooth waveform, then it can be shown that t' is a sample function from a Gaussian process with mean and variance given by

(96) $$E(t') = t_o$$

and

(97) $$\sigma_{t'}^2 = \frac{T_b^2}{4} \frac{\sigma_{V_t}^2}{V_A^2} = \sigma_\epsilon^2 \quad .$$

The timing of the integrate/dump commands are derived from the timing of the trailing edge of each pulse at the comparator output; thus σ_ϵ^2 is the variance of the bit timing error process. The variance σ_ϵ^2 is varied by adjusting the variance of V_t, and the bit timing offset, $\bar{\epsilon}$, is varied by adjusting the phase of the sawtooth waveform with respect to the timing of the received signal Z(t), i.e., the phase of C_j with respect to C_p.

Since V_t is only approximately constant during each decision interval, the length of the integration interval varies slightly with time. To see that this deviation is negligible, consider the following example. Suppose that the normalized standard deviation, $\sigma_{\epsilon n}(= \sigma_\epsilon / T_b)$, is equal to 0.10. Then most values $|\epsilon_n - \bar{\epsilon}_n|$ will be within $3\sigma_{\epsilon n}$. If a sinusoidal time variation of ϵ at a frequency of 2 KHz and an amplitude of $3\sigma_\epsilon$ is assumed, then the maximum variation in the length of an integration interval will be equal to about $(0.01)T_b$, assuming a 50 Kbps data bit rate. This results in a $\pm$ 1% variation in the effective signal power to noise power ratio at the integrator output, a very small deviation. The average variations in the integration interval will be much smaller than $\pm$ 1%. Since the maximum normalized standard deviation considered in this report will be 0.10, the effects of variations in the integration interval will be negligible.

A time interval meter (TIM) is used in conjunction with a digital computer to determine the statistics of the bit timing error. The start and stop commands required to control the TIM are generated using circuits having the block diagrams shown in Fig. 16. Start pulses are generated from the absolute system clock at a rate of six pulses per second. The stop pulses are generated by digitally dividing the frequency of C_j by two. The TIM measures the time interval between the start and stop pulses. Since the TIM can read only positive time intervals, the stop pulse is delayed 20 μsec with respect to the first pulse. The bit timing error is thus related to the TIM reading ($\Delta\tau$) by

$$\epsilon = \Delta\tau - 20 \times 10^{-6} + D \quad . \tag{98}$$

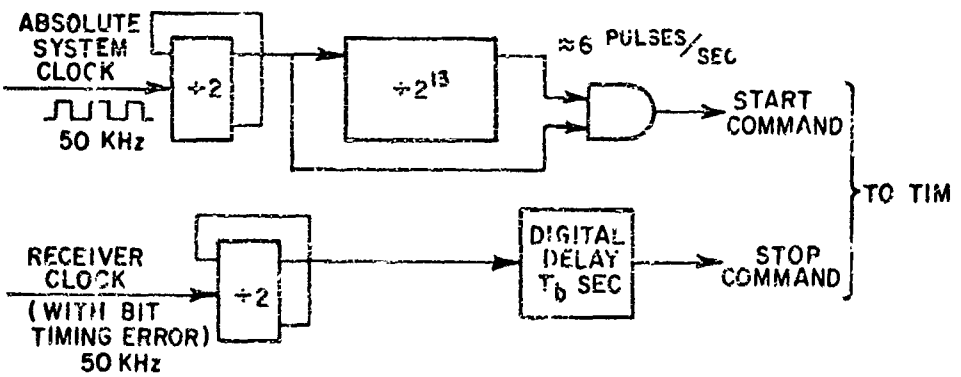

Fig. 16. A block diagram of the bit timing error sampler.

The constant D takes into account delays introduced by the digital and analog circuits. Its value is determined by synchronizing the integrator dump command with the bit transitions at the integrator input, a condition that corresponds to a zero bit timing error. It was found that this point could be determined within an accuracy of $\pm$ 20 nsec. The TIM is accurate within $\pm$10 nsec. The mean ($\bar{\epsilon}$), variance (σ_ϵ^2), and the histogram of the bit timing error process were estimated from 3000 samples of the bit timing error. Histograms for various bit timing jitters showed that the bit timing error process closely approximated a Gaussian process.

The signal to noise ratio was measured using the 30 MHz IF stage of a receiver. The IF bandwidth is nominally equal to 5 KHz and is stable to within $\pm$0.5%. The power of the message carrying component of the received signal, P_r, was measured by removing the biphase modulation and the additive channel noise. Similarly, the noise power was measured (in the 5 KHz bandwidth) by reducing the transmitted power to zero. The bit energy to (single-sided) noise density ratio, E_b/N_o, was then calculated from these measurements.

Two error probabilities, P_E and P_{E_D}, were estimated by averaging each error count over a large number of bit intervals. Each measurement was entered as a data point if: 1) the error count exceeded 100, 2) the number of observed bit intervals exceeded 3×10^6,

and 3) the point was repeatable to within ±1% with respect to the bit energy to noise density ratio.

CHAPTER V
EXPERIMENTAL RESULTS

A. Best Case Performance

The bit error probability of the experimental receiver was measured for the $\Delta f_o = 0$, $\epsilon = 0$, $\delta = 350$ nsec case to determine the effects of extraneous receiver imperfections not included in the mathematical model. These effects include bandlimiting, circuit non-linearities, d.c. offsets, non-zero aperture and acquisition times in the sample/hold circuits, error in matching the gain in each orthogonal channel, error in LO phasing, and measurement error. If all receiver imperfections could be eliminated, the bit error probability versus E_b/N_o would be given by Eq. (23). The measured results, compared to this ideal result, are shown in Fig. 17. Each data point was within 0.17 dB of ideal. From Eq. (24), it can be shown that about 0.075 dB of loss is due to a finite integrator dump time. The remaining 0.095 dB loss is primarily due to the effects of the finite bandwidth B_i and bandlimiting in the integrate/dump and sample/hold circuits (see Appendix C).

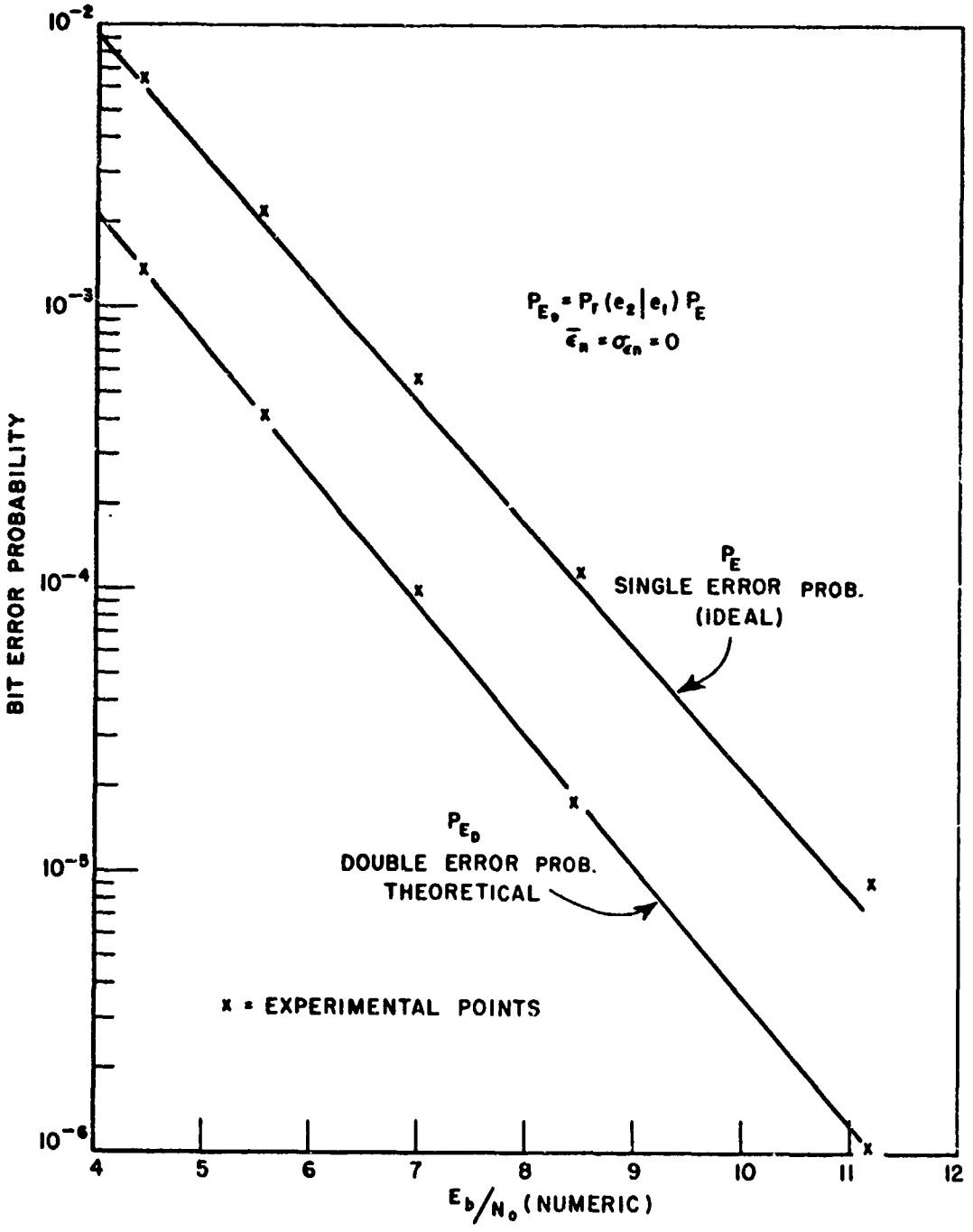

Fig. 17. The bit error probability versus the bit energy to noise density ratio under best case conditions; $\epsilon=0$, $\sigma_\epsilon=0$ and $\Delta f_o=0$. Both analytical and experimental results are given. Analytical and experimental results for the probability of two consecutive errors are also given.

B. Double Error Measurements

The probability of error given that the demodulator erred in the previous bit interval, $P_r(e_m | e_{m-1})$, was determined experimentally as a function of E_b/N_o for $\bar{\epsilon}_n = 0$, $\sigma_{\epsilon n} = 0$, and $\Delta f_o = 0$. The results, given in Fig. 18, compared extremely well with the theoretical result for E_b/N_o in the range 4 to 9 (numeric). The deviation from the

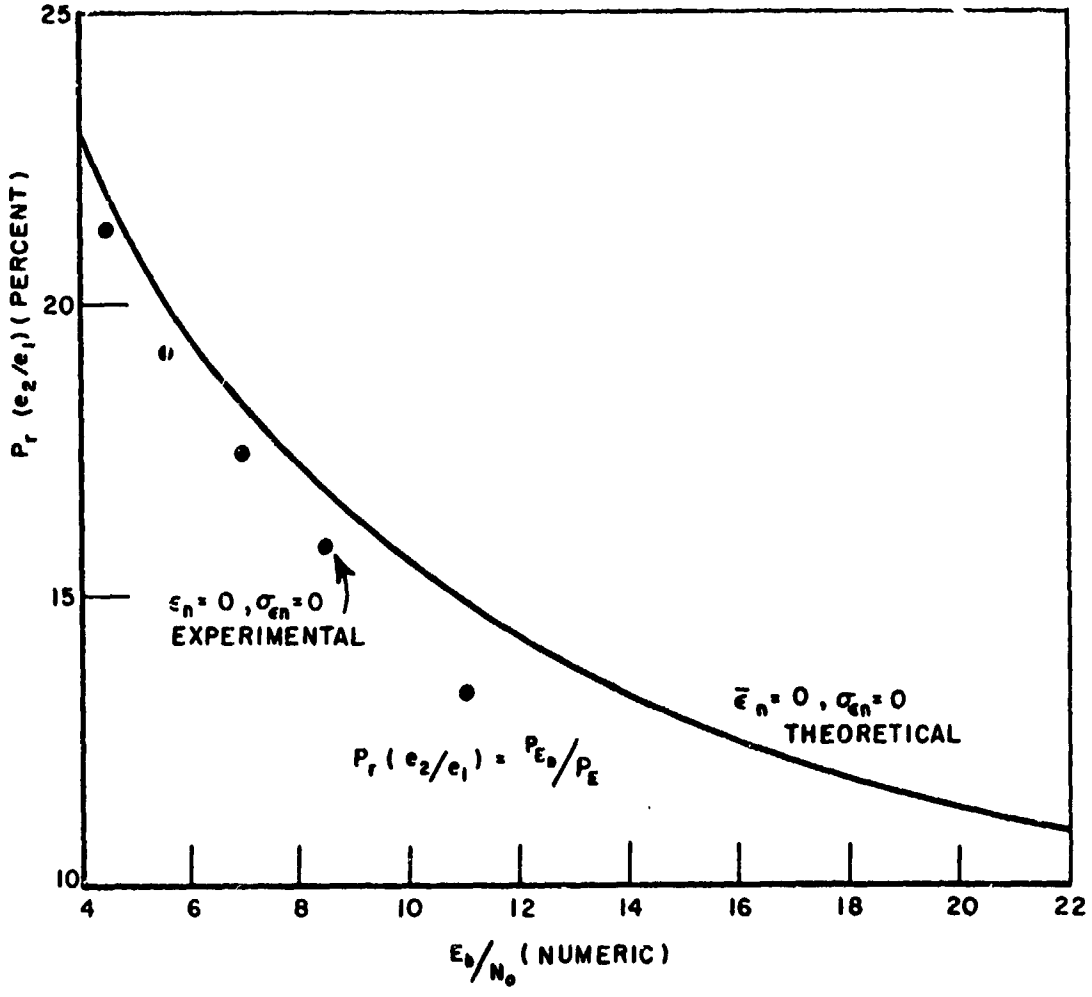

Fig. 18. The probability of error given that an error was detected in the previous bit interval versus the bit energy to noise density ratio for $\epsilon=0$, $\sigma_\epsilon=0$ and $\Delta f_o=0$; both analytical and experimental results are given.

theoretical curve is somewhat larger for the data point corresponding to $E_b/N_o = 11.2$ because the ratio P_{E_D}/P_E is extremely sensitive to receiver imperfections such as intersymbol interference and bandlimiting; that is, at high E_b/N_o, the ratio of the theoretical and measured BEP becomes greater even though the performance difference in terms of E_b/N_o remains approximately the same (see Fig. 17).

C. The Effects of Bit Timing Error

Curves showing the bit error probability as a function of the bit energy to noise density ratio for selected combinations of bit timing offset and bit timing jitter are given in Figs. 19-22; both analytical and experimental results are shown. Again, the analytical and experimental results are in close agreement.

It is recalled that the results of the theoretical analysis showed that the bit error probability was invariant to the sign of the bit timing error. Referring to Fig. 19, it is seen that the measured bit error probability depended on the sign of the bit timing error. This result was due to bandlimiting in the integrate/dump and sample/hold circuits, which had the effect of introducing a 171 nsec delay at the sample/hold output in response to a step applied at the integrator input (see Appendix C). The effect of the delay is illustrated in Fig. 23. When the bit timing error is positive, the overall effect of the delay is to reduce the signal loss that an ideal integrator and sampler would

experience with bit timing error. For a negative bit timing error, the delay causes the signal loss to be greater. Consequently, the BEP was smaller for positive bit timing offsets than for negative bit timing offsets.

Results given in Figs. 20-22 for cases where both the mean and the variance are non-zero apply when the timing offset is negative; thus, they show the detector's performance under worst case conditions. The BEP for $\bar{\epsilon}_n$ positive was slightly lower. Note that for the $\bar{\epsilon}_n = 0$, $\sigma_{\epsilon n} = 0.10$ and the $\bar{\epsilon}_n = 0$, $\sigma_{\epsilon n} = 0.06$ cases, the measured BEP represents the average effect of both positive and negative offsets.

It should also be noted that, when the bit timing error is non-zero, receiver performance may be improved by increasing the dump time δ. For example, consider the effect of dump time when $\bar{\epsilon}_n = \pm 0.08$. If δ is set equal to $0.16\ T_b$, then the bit timing offsets having magnitudes less than $0.08T_b$ do not affect the message carrying component of the integrator outputs. Correspondingly, for $\frac{E_b}{N_o} = 10$ dB, the bit error probability is given by

$$(99) \qquad P_E = \frac{1}{2} \exp\left[- \frac{E_b(T_b - \delta)}{N_o T_b} \right] = 1.11 \times 10^{-4} \ ,$$

Now, the bit error probability for the otherwise ideal differential detector, with $\bar{\epsilon}_n = 0.08$, equals 2.08×10^{-4} -- twice as large as the result in Eq. (99). In certain instances, then, the imperfectly-timed

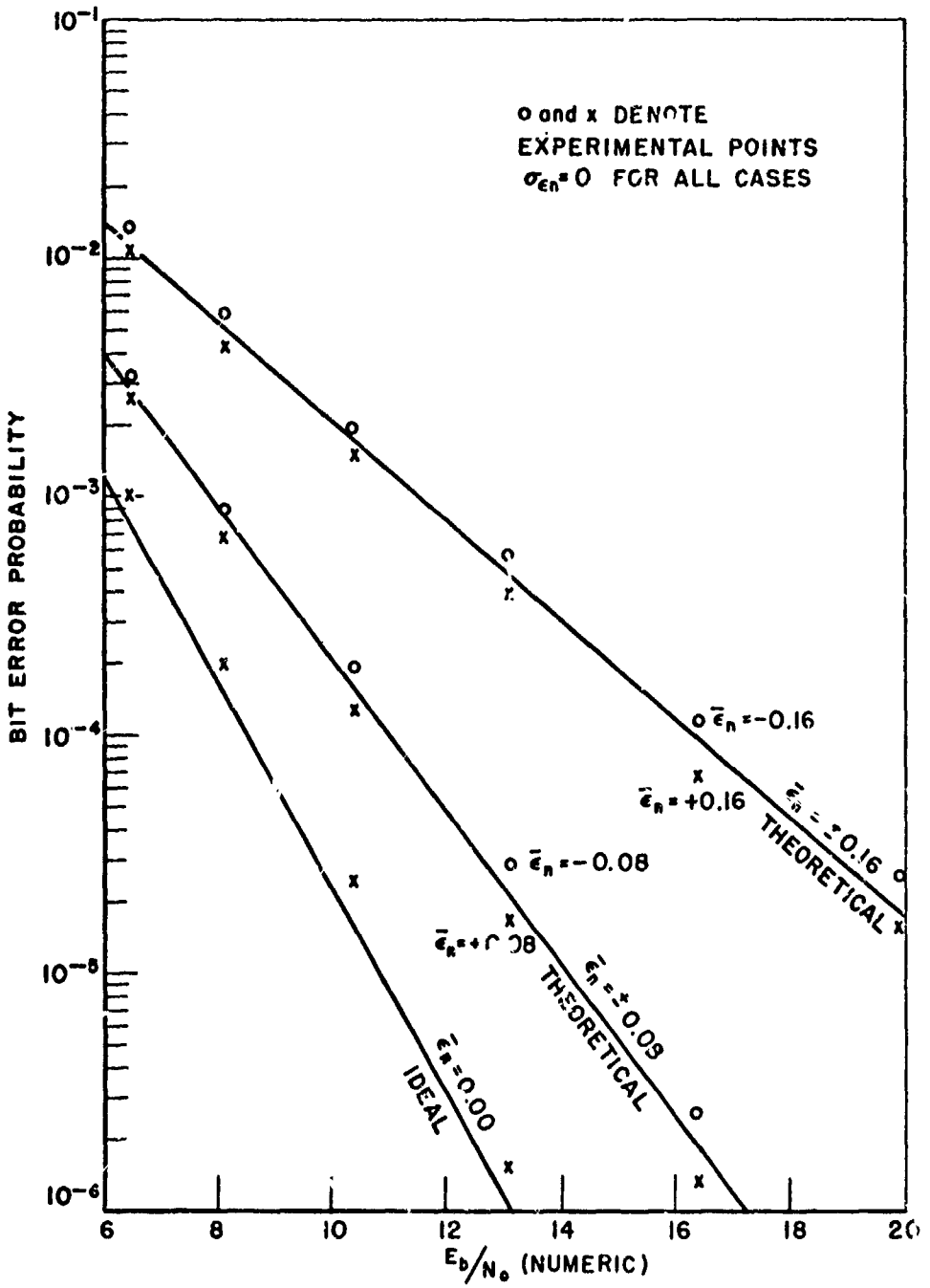

Fig. 19. The bit error probability versus the bit energy to noise density ratio for the imperfectly-timed DD; $\bar{\epsilon}_n=\pm 0.08$ and $\bar{\epsilon}_n=\pm 0.16$. Both analytical and experimental results are given.

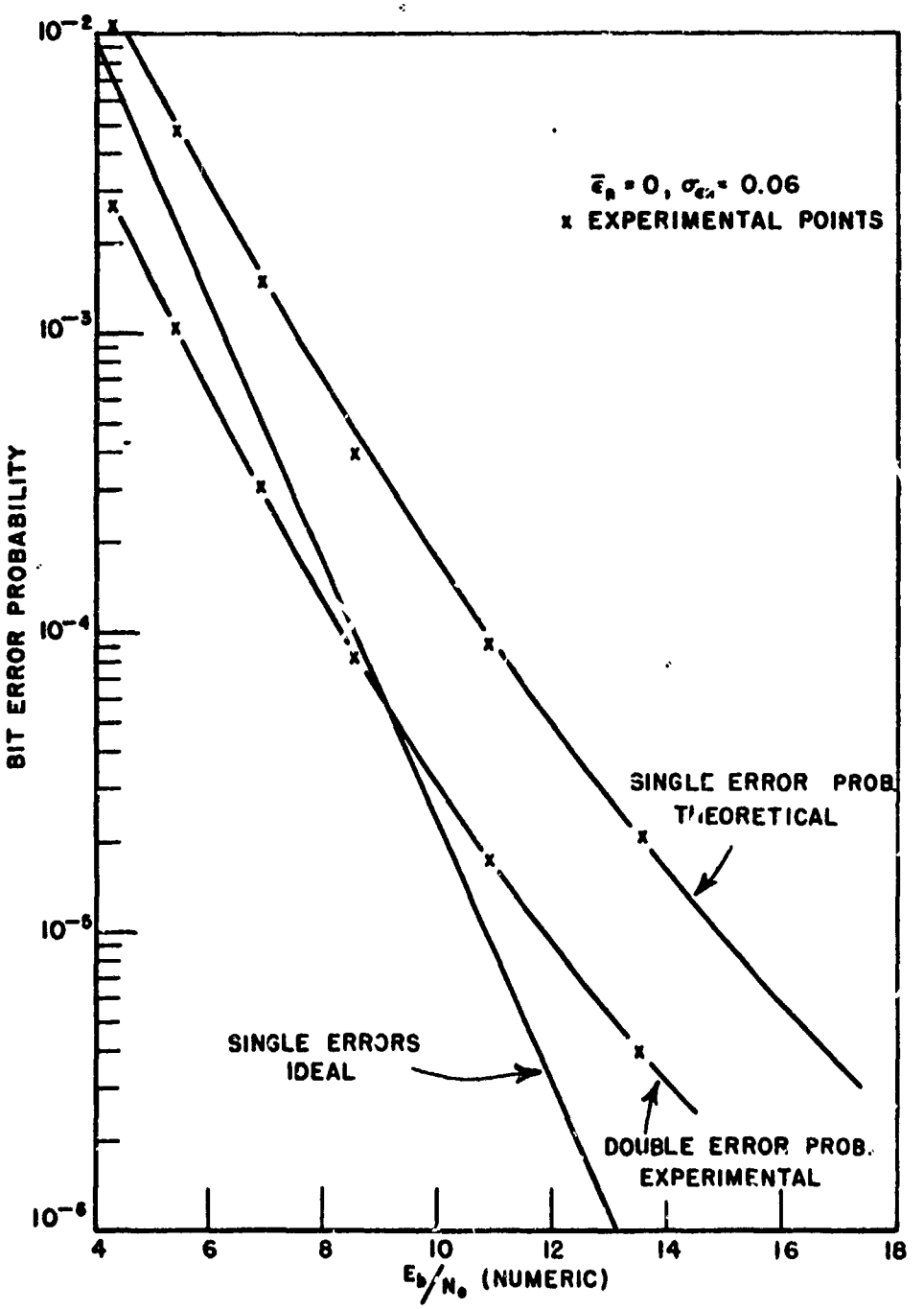

Fig. 20. The bit error probability versus the bit energy to noise density ratio for the imperfectly-timed DD; $\bar{\epsilon}_n=0$ and $\sigma_{\epsilon n}=0.06$. Both analytical and experimental results are given. Nominal experimental results for the probability of two consecutive errors are also given.

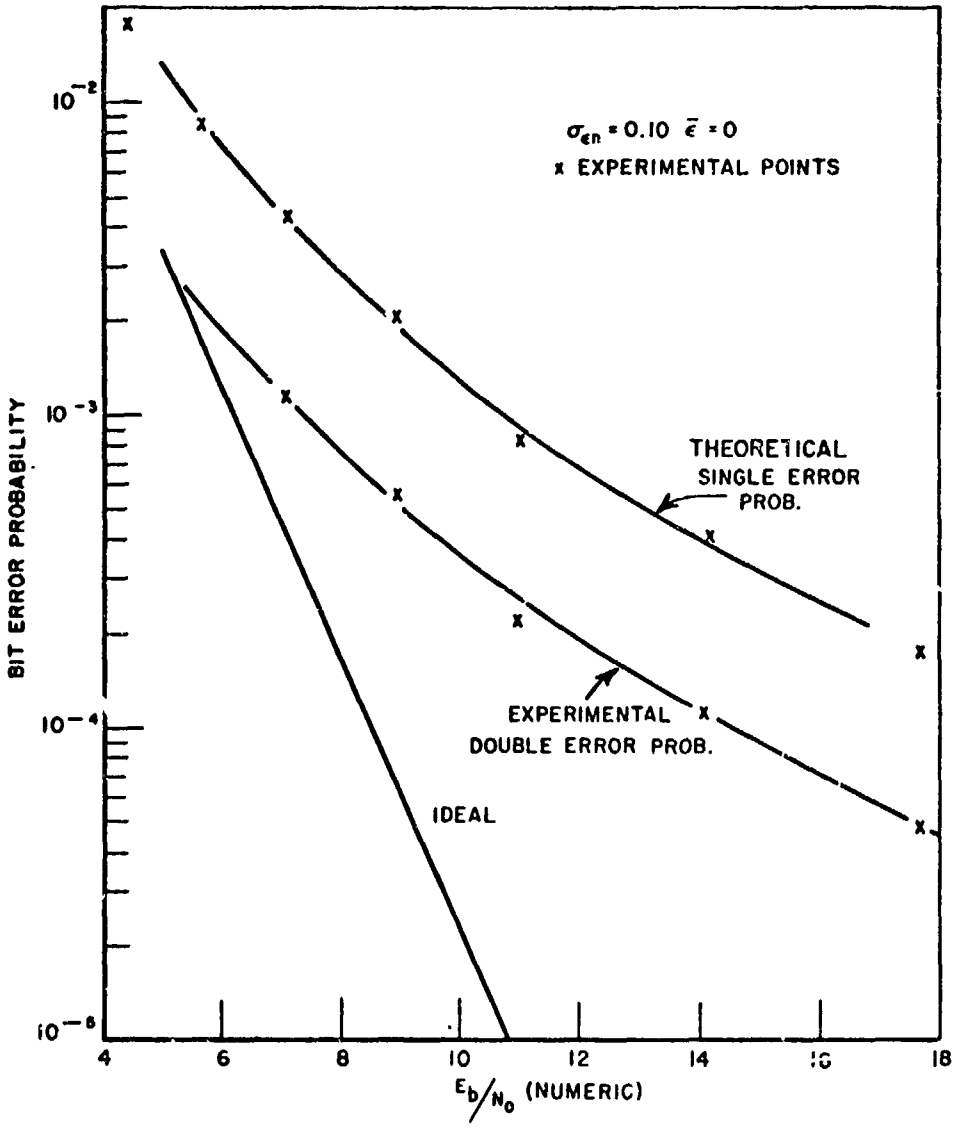

Fig. 21. The bit error probability versus the bit energy to noise density ratio for the imperfectly-timed DD; $\bar{\epsilon}_n$=0 and $\sigma_{\epsilon n}$=0.10. Both analytical and experimental results are given. Nominal experimental results for the probability of two consecutive errors are also given.

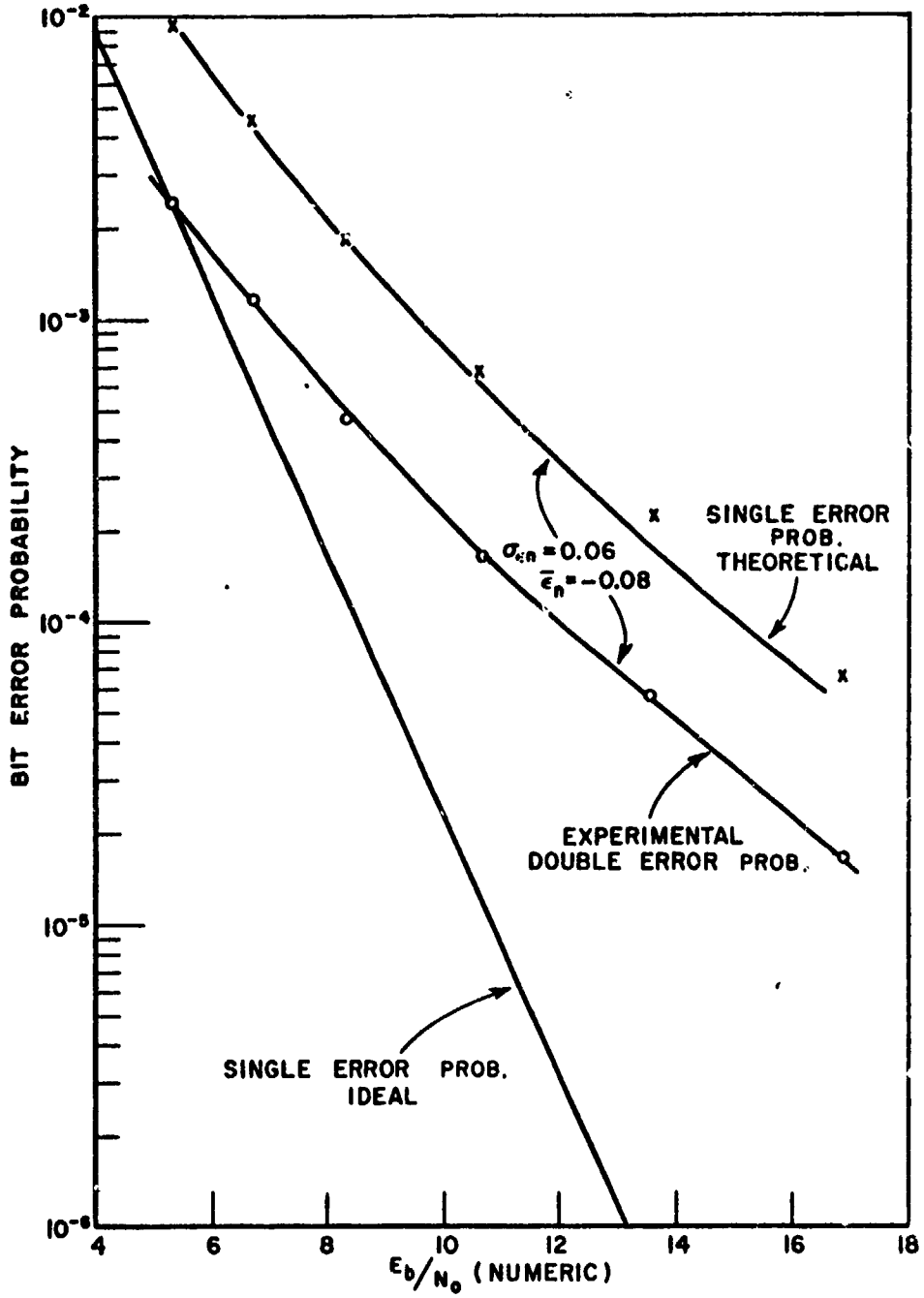

Fig. 22. The bit error probability versus the bit energy to noise density ratio for the imperfectly-timed DD; $\bar{\epsilon}_n = 0.06$ and $\bar{\epsilon}_n = -0.08$. Both analytical and experimental results are given. Nominal experimental results for the probability of two consecutive errors are also given.

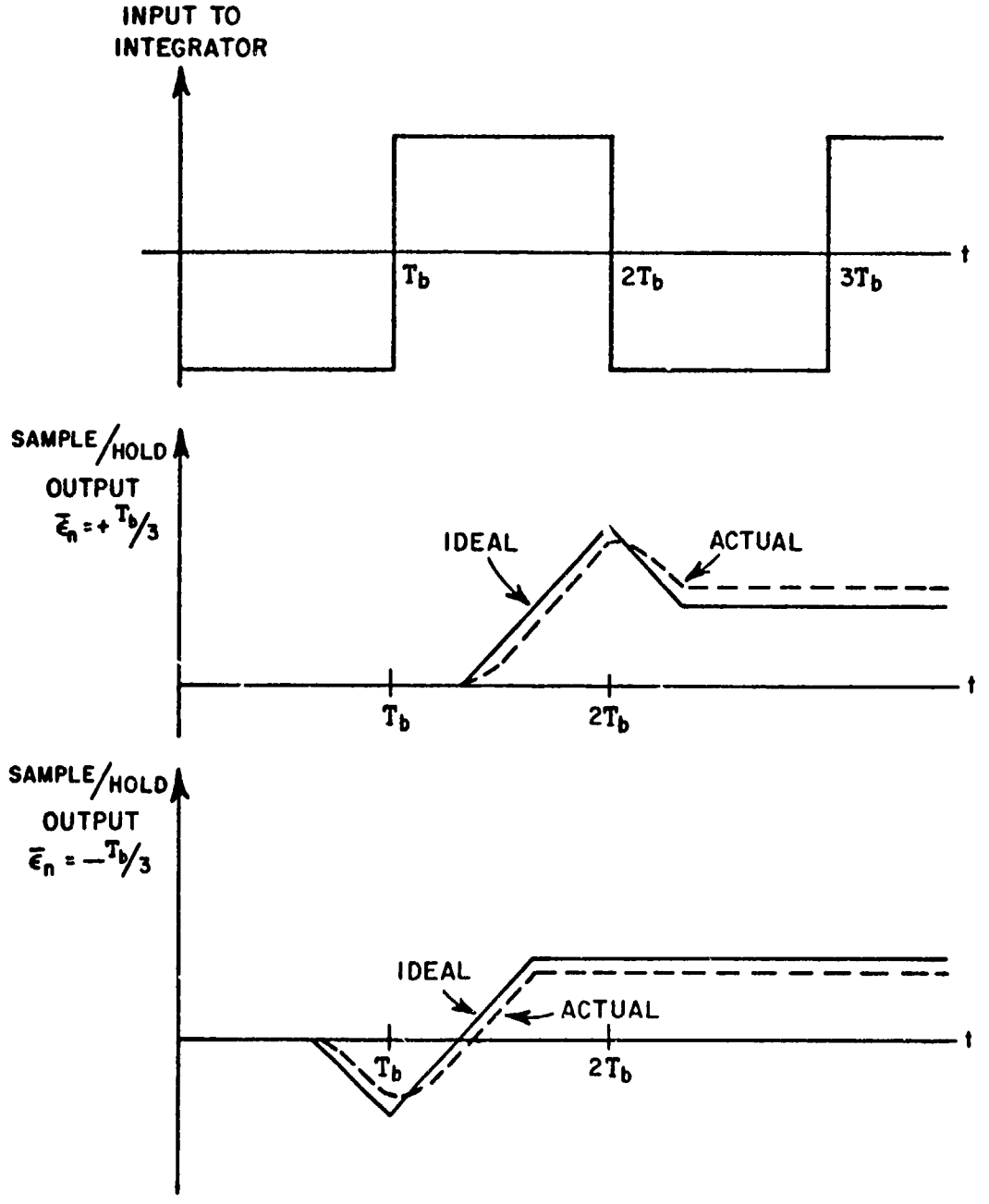

Fig. 23. An example illustrating the effect of bandlimiting in the integrator.

DD will have a lower bit error probability if the dump time is set to some non-zero value.

D. The Effects of Frequency Offset

Curves comparing the measured and analytical BEP as a function of E_b/N_o for selected values of the normalized frequency offset, Δf_η $\left(= \Delta f_o T_b = \frac{\Delta\omega_o T_b}{2\pi}\right)$, are given in Fig. 24. Some experimental and analytical results are also compared, in terms of the ratio μ/μ_o (see p. 38) as a function of E_b/N_o, in Fig. 25.* All experimental results were found to closely agree with analytical results for both positive and negative offsets. In addition, spot measurement results of the BEP for frequency offsets in the range $\pi/2 \leq |\Delta\omega_o T_b| < 3\pi/2$ closely agreed with the bit error probability P_e given by

$$(100) \qquad P_e(\Delta\omega_o, L_1) = u(|\Delta\omega_o T_b| - \pi/2) - \text{sgn}(|\Delta\omega_o T_b| - \pi/2)\, P_E$$

where

$$(101) \qquad u(x) = \begin{cases} 0 & x < 0 \\ 1 & x > 0 \end{cases}$$

$$(102) \qquad \text{sgn}(x) = \begin{cases} -1 & x < 0 \\ +1 & x > 0 \end{cases}$$

*Some of the results shown in Fig. 25 are discussed in the following section.

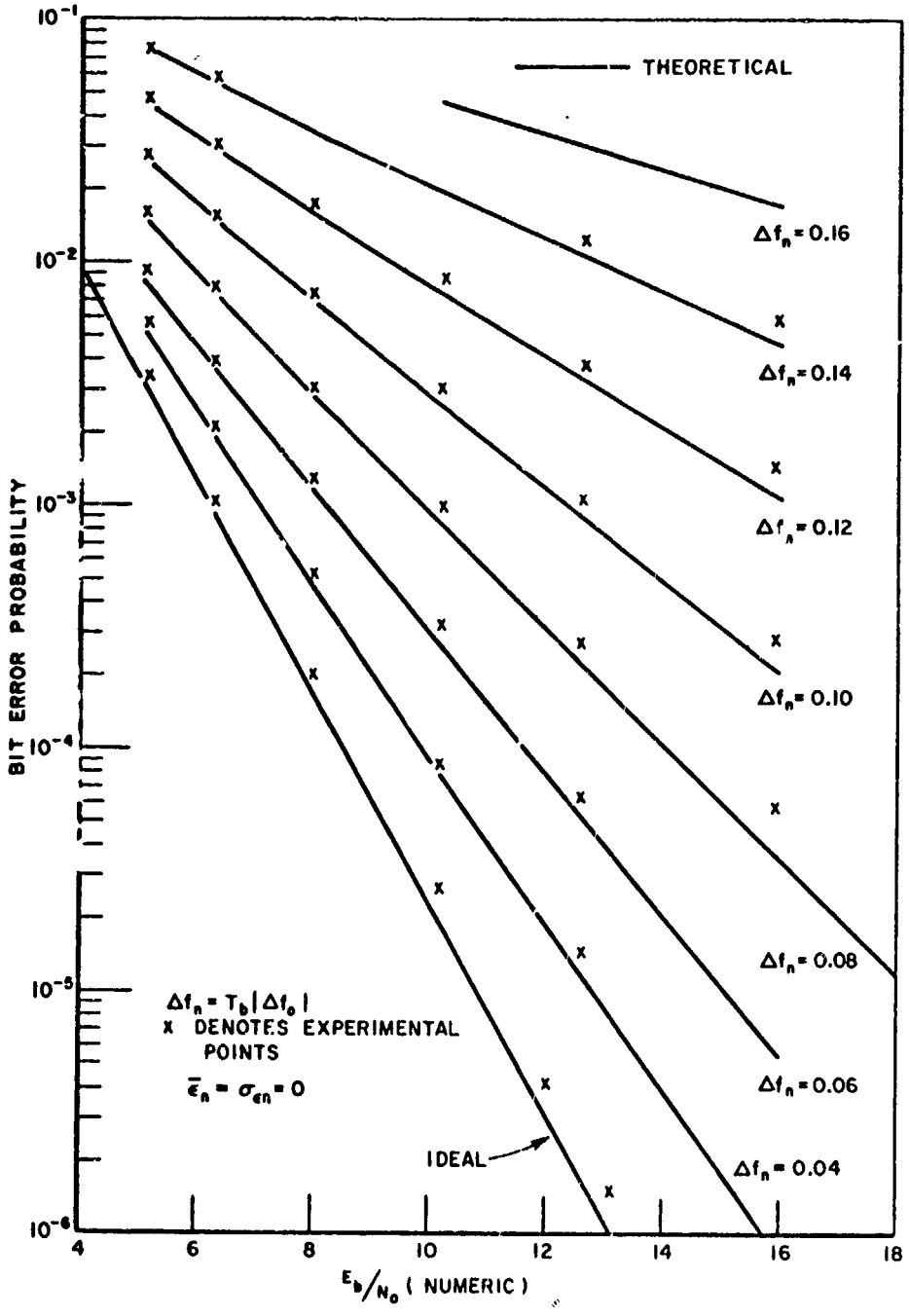

Fig. 24. The bit error probability versus the bit energy to noise density ratio for selected values of frequency offset, both analytical and experimental results are given.

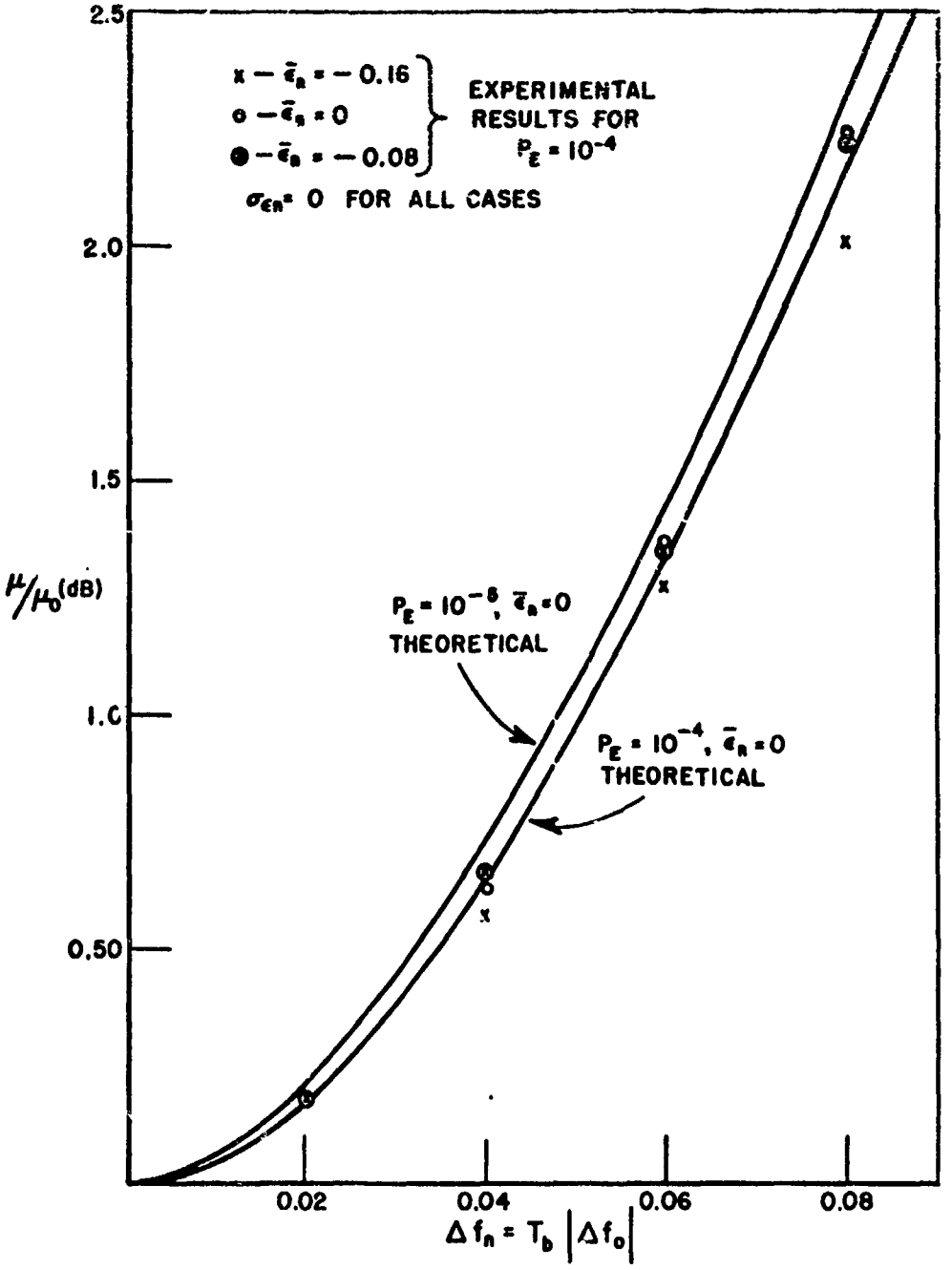

Fig. 25. The ratio μ/μ_0 (see p. 38) versus frequency offset for selected values of the bit error probability; both analytical and experimental results are given for the $\bar{\epsilon}_n = 0$, $\bar{\epsilon}_n = -0.16$, and $\bar{\epsilon}_n = -0.08$ cases.

and P_E is given by Eq. (94), even though the assumption $\Delta\omega_o T_b < \pi/2$ made in the derivation of Eq. (94) is no longer valid. This is due to the fact that the double frequency components in $\xi_x(t)$ and $\xi_y(t)$ are highly attenuated by bandlimiting in the integrate/dump and the sample/hold circuits, a factor not taken into account in the derivation.

E. Additional Experimental Results

The combined effects of frequency offset and bit timing error on the bit error probability and the probability of two consecutive errors are extremely difficult to investigate analytically; for this reason, an experimental investigation was performed. Since the experimental results previously given agreed quite well with available analytical results, the results to be given should accurately reflect receiver performance. Results were obtained showing 1) the combined effects of bit timing error and frequency offset on the BEP, 2) the effect of bit timing error on the probability of two consecutive errors, and 3) the effect of frequency uncertainty on the probability of two consecutive errors.

The combined effects of bit timing error and frequency offset on the BEP as a function of E_b/N_o was determined for selected values of $\overline{\epsilon_n}$; the results are given in Figs. 26 and 27. The performance degradation due to frequency offset for the perfectly and imperfectly timed detectors can be compared by redefining the ratio μ/μ_o (see p. 38) to

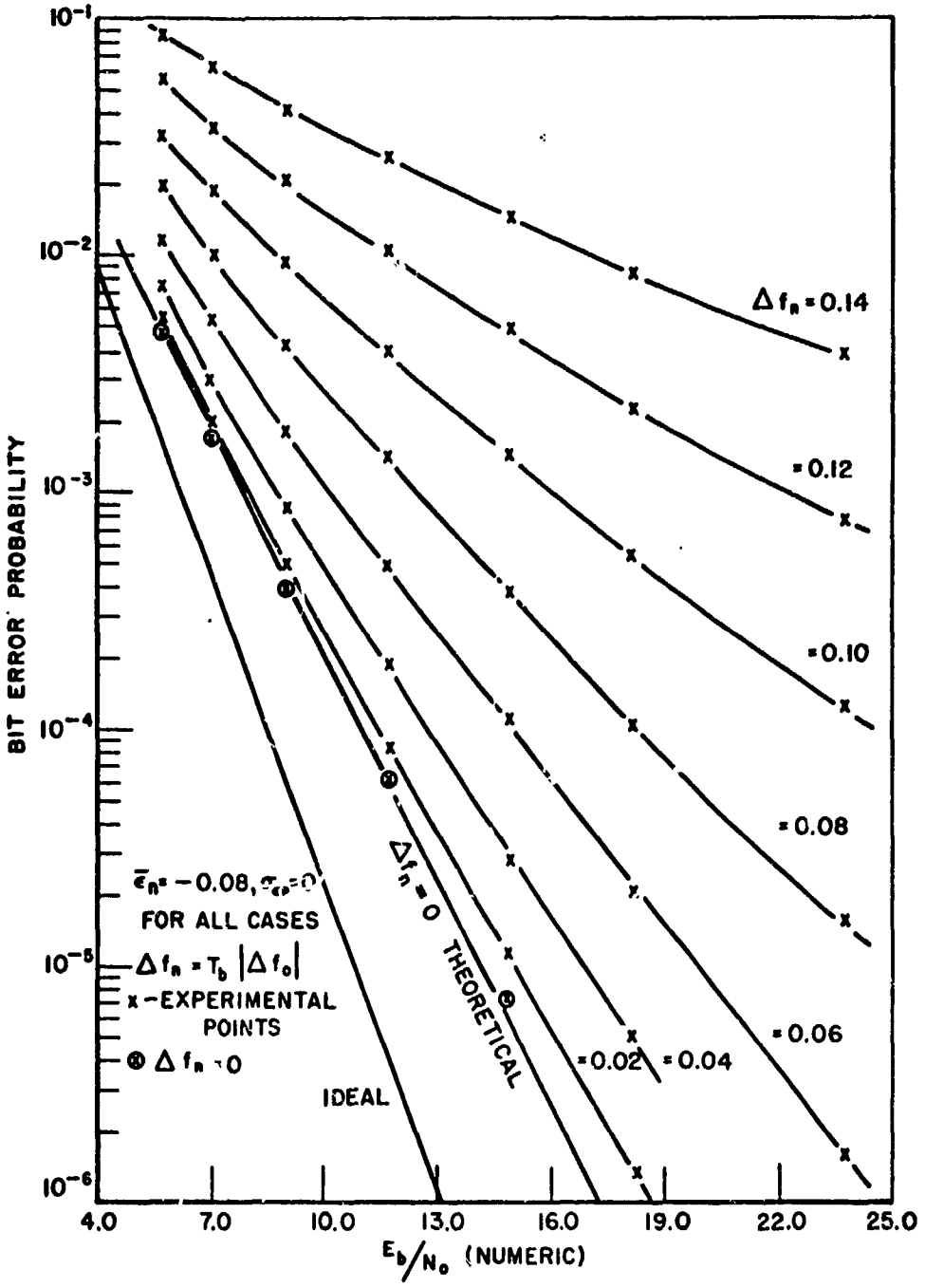

Fig. 26. The bit error probability versus the bit energy to noise density ratio of the imperfectly-timed DD for selected values of the frequency offset; nominal experimental results are given for the $\bar{\epsilon}_n = -0.08$ case.

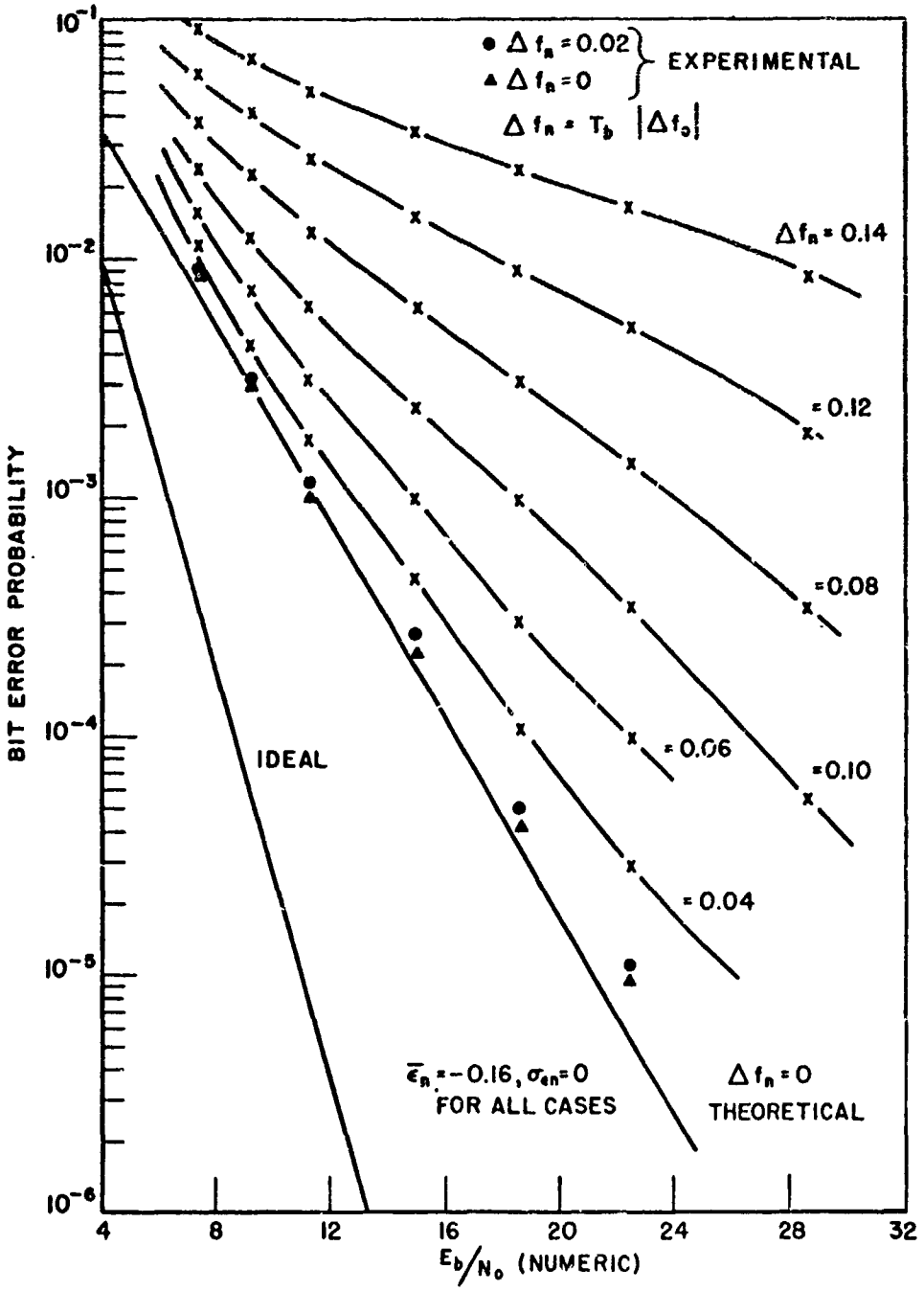

Fig. 27. The bit error probability versus the bit energy to noise density ratio of the imperfectly-timed DD for selected values of the frequency offset; nominal experimental results are given for the $\bar{\epsilon}_n = -0.16$ case.

include the effects of bit timing error. In Fig. 25, measurements of the ratio μ/μ_o are compared to theoretical results for the $\bar{\epsilon}_n = -0.16$ and the $\bar{\epsilon}_n = -0.08$ cases with $P_E = 10^{-4}$. In this figure, μ_o and μ have been defined as the bit energy to noise density ratios required to maintain a given BEP at the output of an imperfectly-timed DD for a zero and non-zero frequency offset, respectively. Note that the normalization factor μ_o is <u>not</u> the same for different bit timing offsets, even though the BEP is the same. The results show that the performance degradation caused by a given frequency offset decreases only slightly even when the bit timing offset is large, e.g., $\bar{\epsilon}_n = -0.16$. This indicates that the ratio μ/μ_o for the imperfectly-timed demodulator can be estimated from the theoretical curves given in Fig. 11.

The probability of two consecutive errors was measured for selected combinations of bit timing jitter and bit timing offset; results are given in Fig. 28 in the form of the ratio $P_r(e_m | e_{m-1}) = \left(\frac{P_{E_D}}{P_E}\right)$ versus E_b/N_o. The results indicate that increases in uncertainty in the bit arrival time leads to increases in the consecutive error ratio. This is a reasonable result, since bit timing error introduces an effective signal to noise ratio loss at the integrator outputs. Again, it was found that $P_r(e_m | e_{m-1})$ decreased as the bit energy to noise density ratio was increased, except for the $\bar{\epsilon}_n = -0.16$ case. For most cases of practical interest, $P_r(e_m | e_{m-1})$ will be less than 25%.

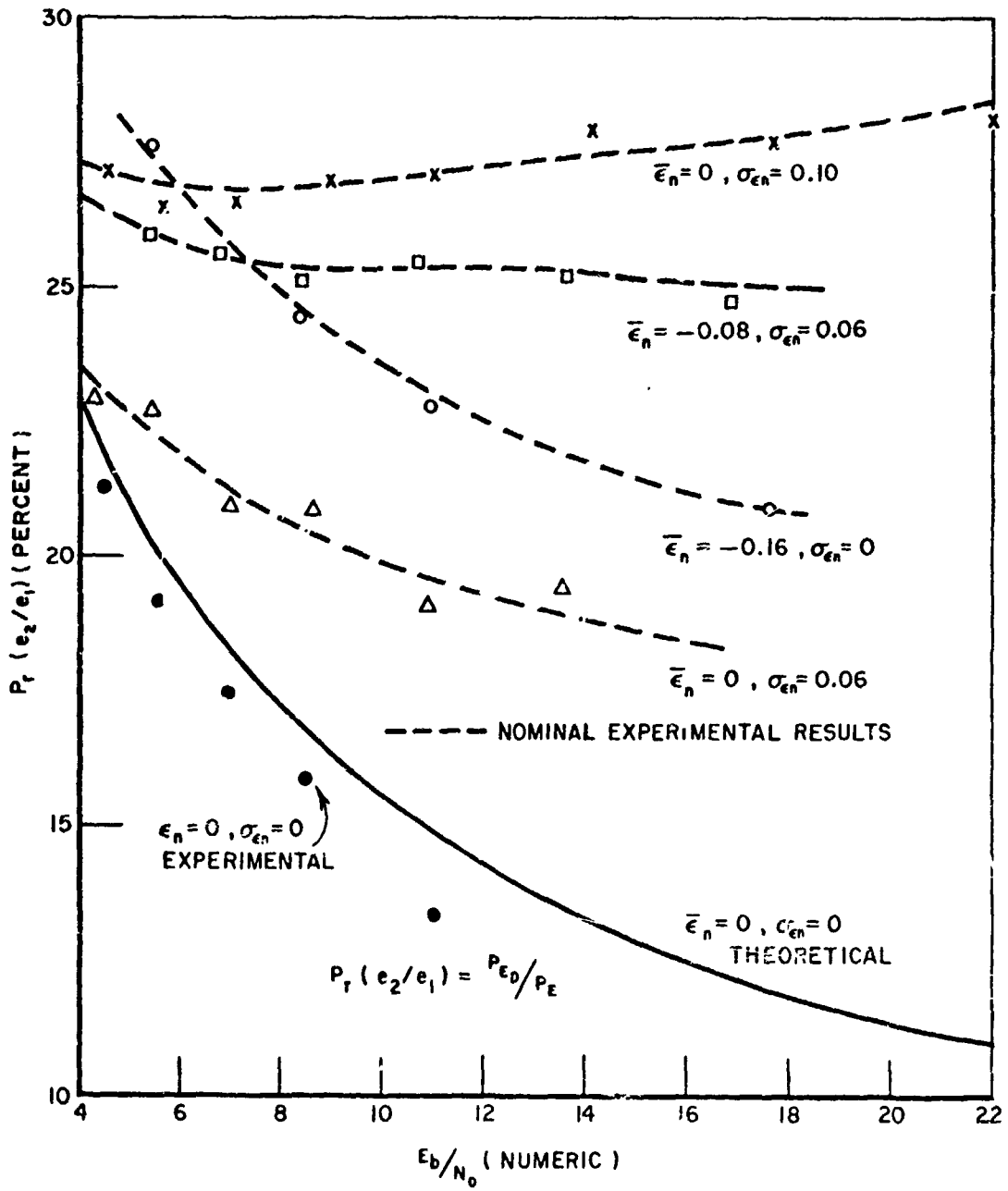

Fig. 28. The probability of error given that an error was detected in the previous bit interval versus the bit energy to noise density ratio for the imperfectly-timed DD. nominal experimental results are given.

The probability of an error given that a detection error occurred in the previous bit interval as a function of frequency offset was measured for selected values of the bit energy to noise density ratio; results are given in Fig. 29. It was found that the ratio $P_r(e_m|e_{m-1})$ decreases rapidly as the frequency offset is increased from zero until a minimum is reached at $\Delta f_n \doteq 0.12$ ($\Delta\omega_o T_b \doteq 0.75$ rad). The measured BEP versus Δf_n is also shown in Fig. 29. Note that, for $|\Delta f_n| \gtrsim 0.09$, the ratio $P_r(e_m|e_{m-1})$ is less than the bit error probability; that is, for normalized frequency offsets greater than 0.09, an error is less likely to occur if a detection error occurred in the previous bit interval. It was also found that the probability of two consecutive errors (P_{E_D}) decreased slightly with increasing frequency offset to a point, as indicated in Fig. 30. For the values of E_b/N_o tested, P_{E_D} reached a minimum value at a normalized frequency offset of about 0.10.

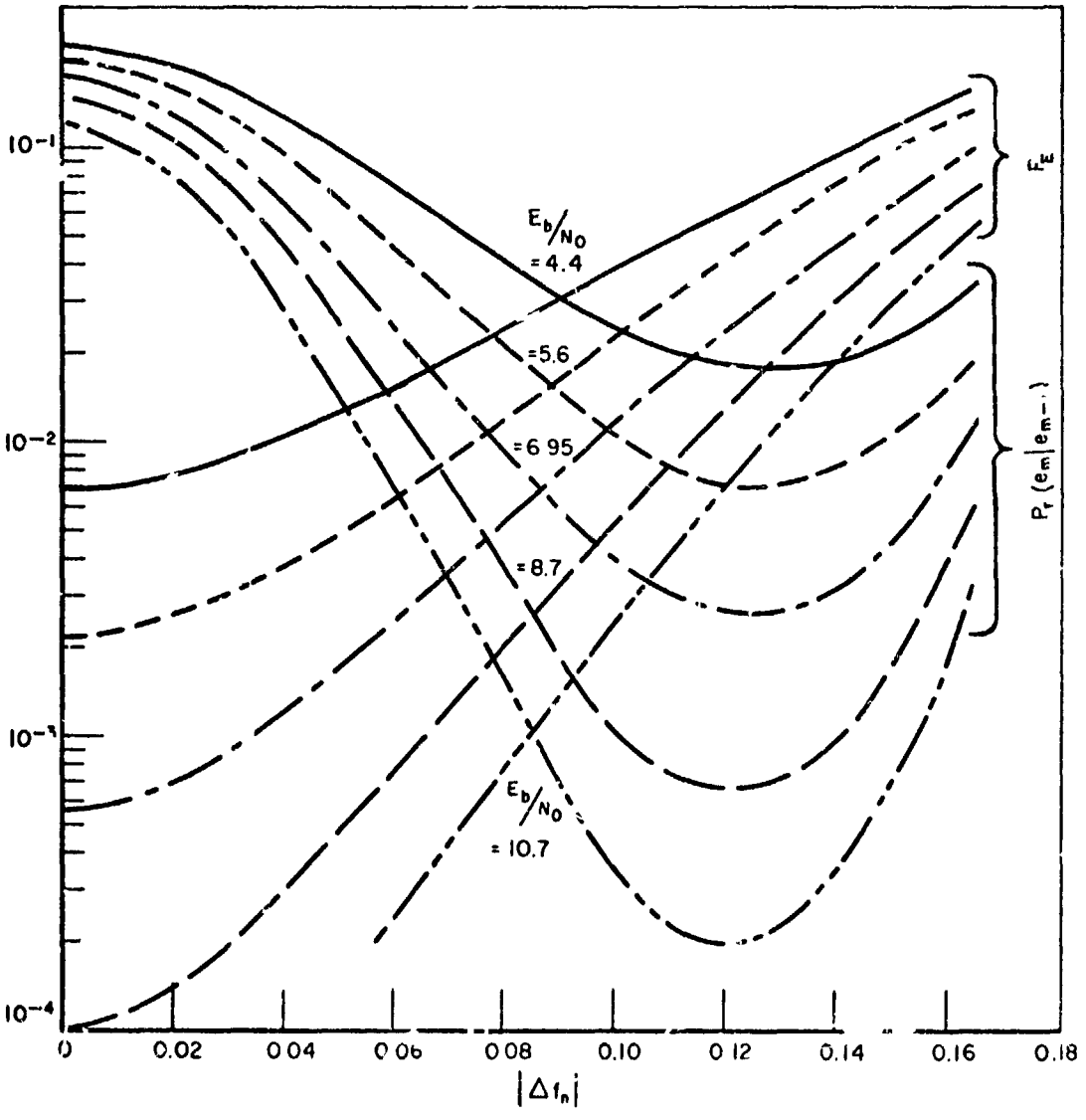

Fig. 29. The probability of error given that an error was detected in the previous bit interval versus frequency offset for selected values of the bit energy to noise density ratio; nominal experimental results are given. Analytical results of the bit error probability for each case are also given.

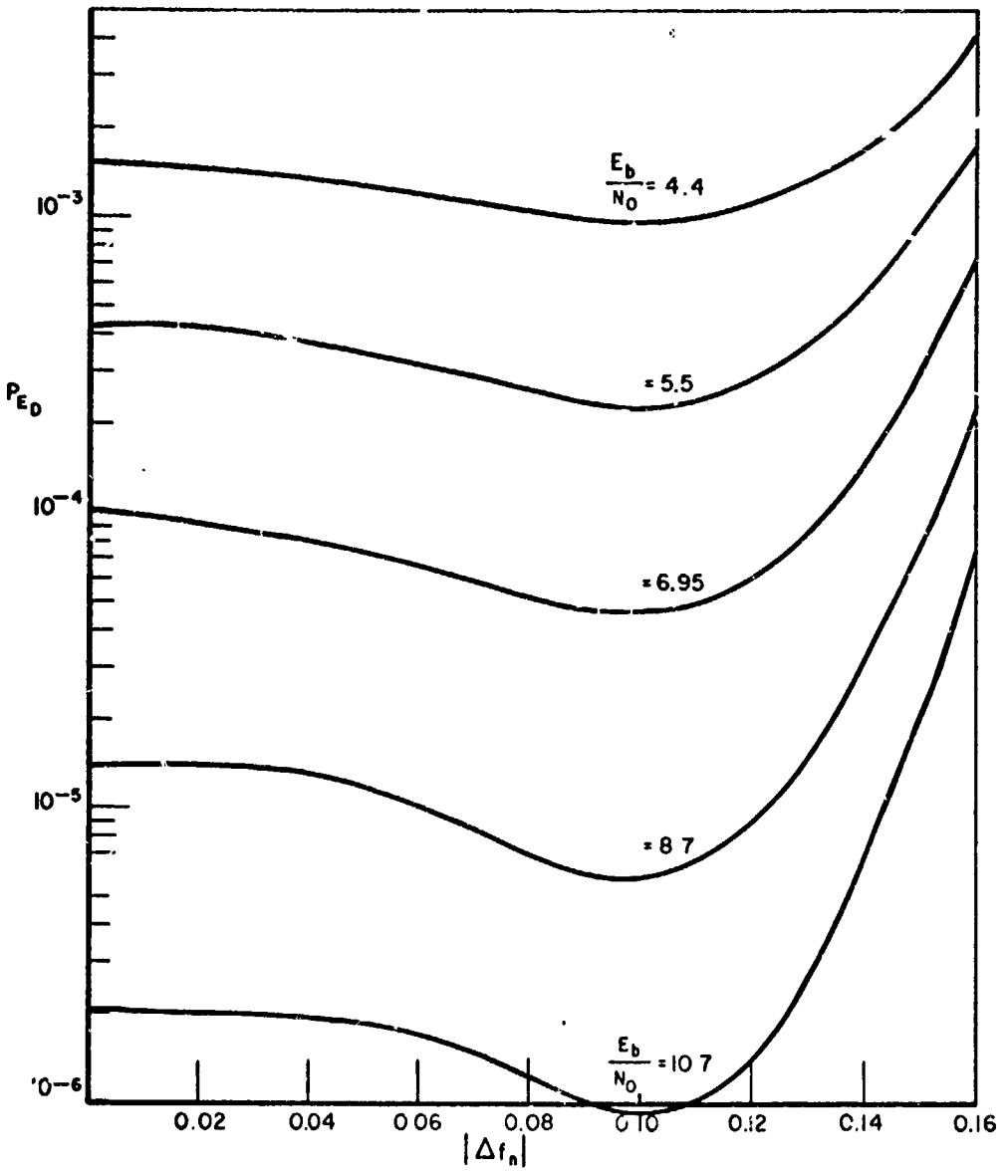

Fig. 30. The probability of two consecutive errors versus frequency offset for selected values of the bit energy to noise density ratio; nominal experimental results are given.

CHAPTER VI
SUMMARY AND CONCLUSIONS

An extensive analytical and experimental investigation of DPSK and differential detection has been presented. The results provide a basis for the design and implementation of a practical differential detector in which changing system geometries are involved, e.g., in a satellite communications link. Available analytical results relating to the performance of the ideal and imperfectly-timed differential detector have been summarized and an expression for the bit error probability in cases where the estimate of the carrier frequency is in error has been derived and numerical results documented. To check the accuracy of analytical results, an experimental differential detector was implemented. The details of the detector's construction have been described and its performance documented. The experimental results were found to closely agree with available analytical results and with the result derived relating to the effects of frequency uncertainty. It is concluded that the analytical results presented in this report can be applied to practical DPSK systems with confidence and that the experimental results obtained for cases in which no analytical results are available accurately reflect demodulator performance.

APPENDIX A
A COMPARISON OF IDEAL COHERENT AND IDEAL DIFFERENTIAL DETECTORS

If the additive channel noise is a zero mean white Gaussian process and antipodal modulation is employed, then the bit error probabilities for ideal PSK, ideal DC-PSK, and ideal DPSK (using differential detection) are given by

(103) $$P_e = \frac{1}{2} \operatorname{erfc} \left[\sqrt{\frac{E_b}{N_o}} \right] \quad \text{for PSK[7, 13]}$$

(104) $$P_{ec} = 2 P_e(1 - P_e) \quad \text{for DC-PSK[5]}$$

and

(105) $$P_E = \frac{1}{2} \exp \left[- \frac{E_b}{N_o} \right] \quad \text{for DPSK[6, 7, 9]} \quad .$$

Curves showing the additional signal energy required for ideal differential detection to maintain a BEP equal to that of an ideal coherent detector and for an ideal differentially-coded coherent detector, as a function of the bit energy to noise density ratio at the input to the coherent detector, is given in Fig. 31. At $\frac{E_b}{N_o} = 10$ dB, the ideal coherent detector performs only 0.70 better than the ideal DD. This is significant in that the DD does not require a phase reference.

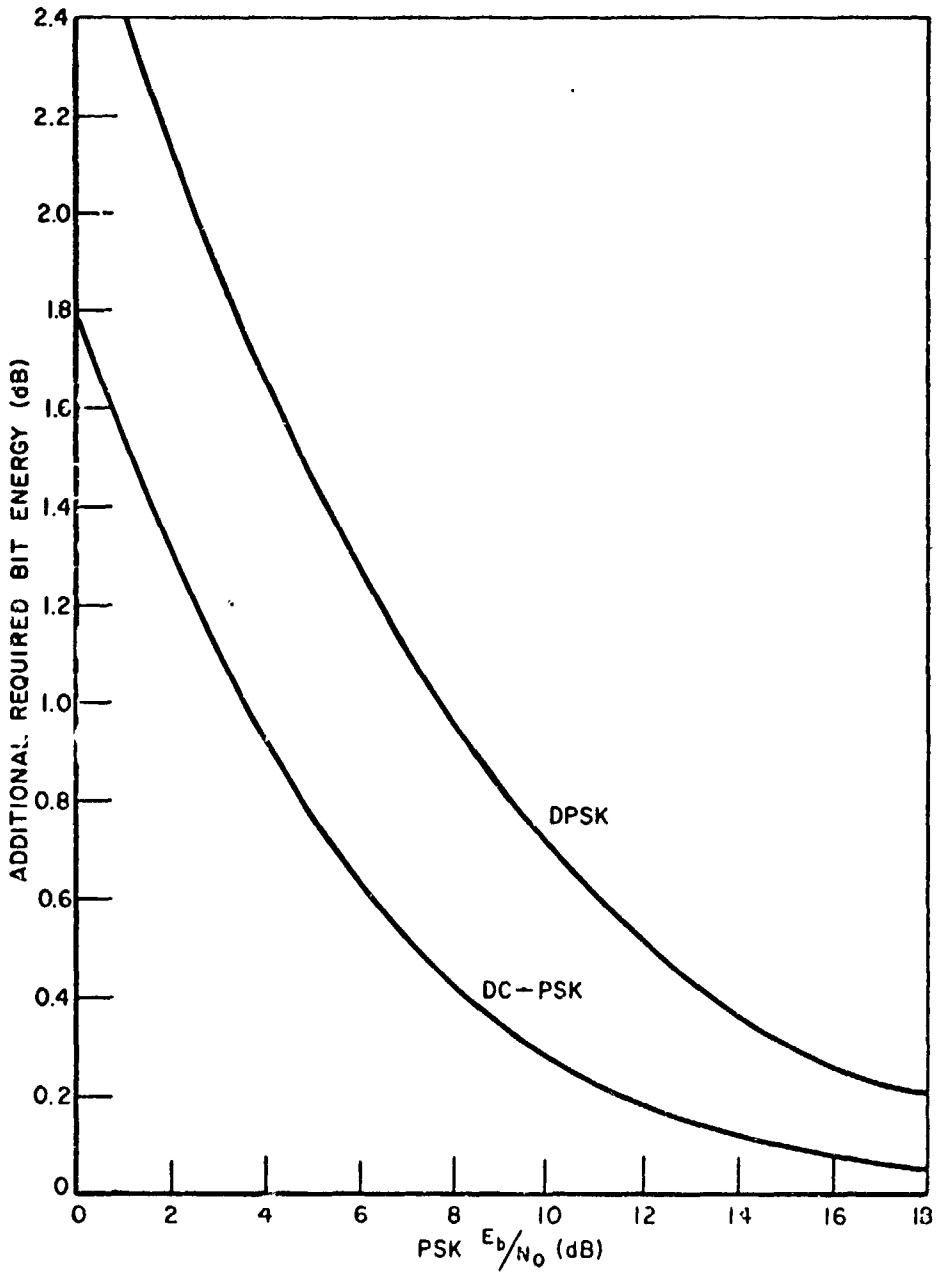

Fig. 31. A comparison of ideal differential detection, ideal differentially-coded coherent detection, and ideal coherent detection.

APPENDIX B
CALCULATIONS

The following expression for P_E is to be simplified to facilitate numerical evaluation:

$$P_E = \frac{1}{2} \exp\left[-\frac{L_1^2}{N_o}\right] + E_1 - E_2 \tag{106}$$

where

$$E_1 = \frac{2L_1}{\sqrt{\pi N_o}} \int_0^{\pi/2} Q(L_1, \psi_1) \exp\left[-\frac{L_1^2 \sin^2\psi_1}{N_o}\right] \cos\psi_1 \, d\psi_1 \tag{107}$$

$$E_2 = \frac{L_1}{2\sqrt{\pi N_o}} \int_{-\pi}^{\pi} Q(L_1, \Delta\omega_o T_b - \psi) \exp\left[-\frac{L_1^2 \sin^2\psi}{N_o}\right] \cos\psi \, d\psi \ .$$

The integral E_2 will first be evaluated. It can easily be shown that

$$E_2 = \frac{L_1}{2\pi\sqrt{2N_o}} \int_{-\pi}^{\pi} \int_0^{L_1\sqrt{\frac{2}{N_o}}\cos(\Delta\omega_o T_b - \psi)} \exp\left[-\frac{u^2}{2}\right] du \cdot \exp\left[-\frac{L_1^2 \sin^2\psi}{N_o}\right] \cos\psi \, d\psi \tag{108}$$

$$= \frac{L_1}{2\pi\sqrt{2N_o}} \int_{-\pi}^{\pi} \int_0^{L_1\sqrt{\frac{2}{N_o}}\cos(\psi \pm \Delta\omega_o T_b)} \exp\left[-\frac{u^2}{2}\right] du \cdot \exp\left[-\frac{L_1^2 \sin^2\psi}{N_o}\right] \cos\psi \, d\psi \ .$$

Therefore, E_2 is invariant to the sign of the frequency offset. Also, it is easy to show that

$$(109) \qquad \int_{\pi/2}^{\pi} \xi(\psi, \Delta\omega_o)d\psi = \int_{-\pi/2}^{0} \xi(\psi, \Delta\omega_o)d\psi$$

and

$$(110) \qquad \int_{0}^{\pi/2} \xi(\psi, \Delta\omega_o)d\psi = \int_{-\pi}^{-\pi/2} \xi(\psi, \Delta\omega_o)d\psi$$

where

$$(111) \qquad \xi(\psi, \Delta\omega_o) = \int_0^{L_1\sqrt{\frac{2}{N_o}}\cos(\psi+\Delta\omega_o T_b)} \exp\left[-\frac{u^2}{2}\right] du \cdot \exp\left[-\frac{L_1^2\sin^2\psi}{N_o}\right]\cos\psi \ .$$

Thus,

$$(112) \qquad E_2 = \frac{L_1}{\pi\sqrt{2N_o}} \int_{-\pi/2}^{\pi/2} \xi(\psi, \Delta\omega_o)d\psi$$

$$= \frac{L_1}{\pi\sqrt{2N_o}} \left[\int_0^{\pi/2} (\xi(\psi, \Delta\omega_o) + \xi(-\psi, \Delta\omega_o))\, d\psi\right]$$

$$= \frac{L_1}{\pi\sqrt{2N_o}} \left\{\int_0^{\pi/2} \left[2\int_0^{L_1\sqrt{\frac{2}{N_o}}\cos x \cos\Delta\omega_o T_b} \exp\left[-\frac{v^2}{2}\right] du \cdot \exp\left[-\frac{L_1^2\sin^2 x}{N_o}\right]\cos x\right.\right.$$

(cont.)

(112) (cont.)

$$+\int_{L_1\sqrt{\frac{2}{N_o}}\cos x\cos\Delta\omega_o T_b}^{L_1\sqrt{\frac{2}{N_o}}\cos(x+\Delta\omega_o T_b)} \exp\left[-\frac{u^2}{2}\right] du \cdot \exp\left[-\frac{L_1^2\sin^2 x}{N_o}\right]\cos x$$

$$+\int_{L_1\sqrt{\frac{2}{N_o}}\cos x\cos\Delta\omega_o T_b}^{L_1\sqrt{\frac{2}{N_o}}\cos(x-\Delta\omega_o T_b)} \exp\left[-\frac{u^2}{2}\right] du \cdot \exp\left[-\frac{L_1^2\sin^2 x}{N_o}\right]\cos x\,dx\Bigg\} .$$

By using the relation[1]

$$(113)\qquad \frac{2A}{\pi\sqrt{2N_o}}\int_0^{\pi/2}\int_0^{B\sqrt{\frac{2}{N_o}}\cos\psi_1} \exp\left\{-\left[\frac{u^2}{2}+\frac{A^2\sin^2\psi_1}{N_o}\right]\right\} du\cos\psi_1\, d\psi_1$$

$$= \frac{1}{2} - \frac{1}{\pi}\int_0^{\pi/2} \exp\left[\frac{-A^2B^2/N_o}{A^2\cos^2\theta + B^2\sin^2\theta}\right] d\theta$$

and by letting $A = L_1$ and $B = L_1\cos\Delta\omega_o T_b = L_2$, the first term in Eq. (112) reduces to

$$(114)\qquad \frac{2L_1}{\pi\sqrt{2N_o}}\int_0^{\pi/2}\int_0^{L_1\sqrt{\frac{2}{N_o}}\cos x\cos\Delta\omega_o T_b} \exp\left[-\left(\frac{u^2}{2}+\frac{L_1^2\sin^2 x}{N_o}\right)\right] du \cdot \cos x\,dx$$

$$= \frac{1}{2} - \frac{1}{\pi}\int_0^{\pi/2} \exp\left[-\frac{L_1^2L_1^2\cos^2\Delta\omega_o T_b}{L_1^2\cos^2\theta + L_1^2\cos^2\Delta\omega_o T_b\sin^2\theta}\right] d\theta$$

$$= \frac{1}{2} - \frac{1}{\pi}\int_0^{\pi/2} \exp\left[-\frac{L_1^2L_2^2}{L_1^2\cos^2\theta + L_2^2\sin^2\theta}\right] d\theta .$$

Consequently,

$$(115)\qquad E_2 = \frac{1}{2} - \frac{1}{\pi}\int_0^{\pi/2} \exp\left[-\frac{L_1^2 L_2^2/N_o}{L_1^2\cos^2\theta + L_2^2\sin^2\theta}\right] d\theta$$

$$+ \frac{L_1}{\pi\sqrt{2N_o}}\int_0^{\pi/2}\int_{L_1\sqrt{\frac{2}{N_o}}\cos x\cos\Delta\omega_o T_b}^{L_1\sqrt{\frac{2}{N_o}}\cos(x+\Delta\omega_o T_b)} \exp\left[-\frac{u^2}{2}\right] du \cdot \exp\left[-\frac{L_1^2\sin^2 x}{N_o}\right]\cos x\, dx$$

$$+ \frac{L_1}{\pi\sqrt{2N_o}}\int_0^{\pi/2}\int_{L_1\sqrt{\frac{2}{N_o}}\cos x\cos\Delta\omega_o T_b}^{L_1\sqrt{\frac{2}{N_o}}\cos(x-\Delta\omega_o T_b)} \exp\left(-\frac{u^2}{2}\right) du \cdot \exp\left[-\frac{L_1^2\sin^2 x}{N_o}\right]\cos x\, dx .$$

In the final form, E_2 simplifies to

$$(116)\qquad E_2 = \frac{1}{2} - \frac{1}{\pi}\int_0^{\pi/2} \exp\left[-\frac{L_1^2 L_2^2/N_o}{L_1^2\cos^2\theta + L_2^2\sin^2\theta}\right] d\theta$$

$$+ \frac{L_1}{\pi\sqrt{2N_o}}\int_{-\pi/2}^{\pi/2}\int_{L_1\sqrt{\frac{2}{N_o}}\cos x\cos\Delta\omega_o T_b}^{L_1\sqrt{\frac{2}{N_o}}\cos(x+\Delta\omega_o T_b)} \exp\left[-\frac{u^2}{2}\right] du \cdot \exp\left[-\frac{L_1^2\sin^2 x}{N_o}\right]\cos x\, dx .$$

Utilizing the technique employed by Huff[1], it can be shown that E_1, given by

$$(117) \qquad E_1 = \frac{2L_1}{\sqrt{\pi N_o}} \int_0^{\pi/2} \frac{1}{\sqrt{2\pi}} \int_0^{L_1\sqrt{\frac{2}{N_o}}\cos\psi} \exp\left[-\frac{u^2}{2}\right] du \cdot \exp\left[-\frac{L_1^2 \sin^2\psi_1}{N_o}\right] \cos\psi_1 \, d\psi_1$$

simplifies to

$$(118) \qquad E_1 = \frac{1}{2} - \frac{1}{2} \exp\left[-\frac{L_1^2}{N_o}\right] .$$

Thus,

$$(119) \qquad P_E = \frac{1}{\pi} \int_0^{\pi/2} \exp\left[-\frac{L_1^2 L_2^2/N_o}{L_1^2 \cos^2\theta + L_2^2 \sin^2\theta}\right] d\theta$$

$$- \frac{L_1}{\pi\sqrt{2N_o}} \int_{-\pi/2}^{\pi/2} \int_{L_1\sqrt{\frac{2}{N_c}}\cos\psi\cos\Delta\omega_o T_b}^{L_1\sqrt{\frac{2}{N_o}}\cos(\psi+\Delta\omega_o T_b)} \exp\left[-\frac{u^2}{2}\right] du \cdot \exp\left[-\frac{L_1^2 \sin^2\psi_1}{N_o}\right] \cos\psi \, d\psi .$$

APPENDIX C
THE INTEGRATE/DUMP AND SAMPLE/HOLD CIRCUITS

A. The Integrate/Dump Circuit

A schematic diagram of the integrate/dump circuit employed in the DD is given in Fig. 32. The circuit was designed to provide accurate integration for small values of time and to have a very short dump time capability. To evaluate actual performance, the integrator will be analyzed for the short integration interval case.

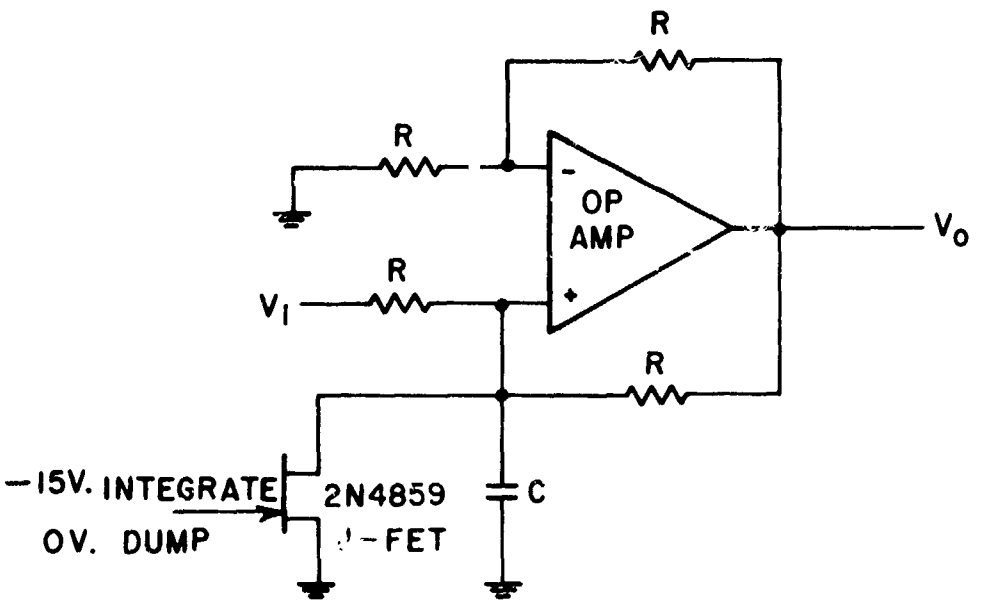

Fig. 32. A schematic diagram of the integrate/dump circuit employed in the DD.

If the operational amplifier in Fig 32 is assumed to be ideal, e.g., if infinite gain, bandwidth, and input impedance is assumed, then the output voltage $V_o(t)$ is given by

$$(120) \qquad V_o(t) = \frac{2}{RC} \int_0^{T_b} V_i \, dt \quad .$$

In practice, the open loop gain, bandwidth, and input impedance are finite. For example, the transfer function of most operational amplifiers has a 6 dB/octave rolloff at high frequencies, as illustrated in Fig. 33. On assuming that the input impedance is infinite, that the input bias current and voltage offset are negligible, and that the amplifier has the transfer function given in Fig. 33, it can be shown that the transfer function $\frac{V_o}{V_i}(S)$ is given by

$$(121) \qquad \frac{V_o}{V_i}(S) = \frac{\frac{R_o}{AR} + 1}{2\frac{R_o}{A_o R} + \frac{2}{A_o} + \left(\frac{3R_oC}{2A_o} + \frac{1}{\pi f_T} + \frac{RC}{A_o} + \frac{RC}{2}\right)S + \frac{RC}{2\pi f_T} S^2}$$

where A_o represents the open loop d.c. gain, f_T the small signal unity gain bandwidth, and R_o the open loop output resistance. If, in addition, it is assumed that

$$(122) \qquad \frac{3R_o}{A_o R} << 1$$

$$(123) \qquad \pi RCf_T >>> 1$$

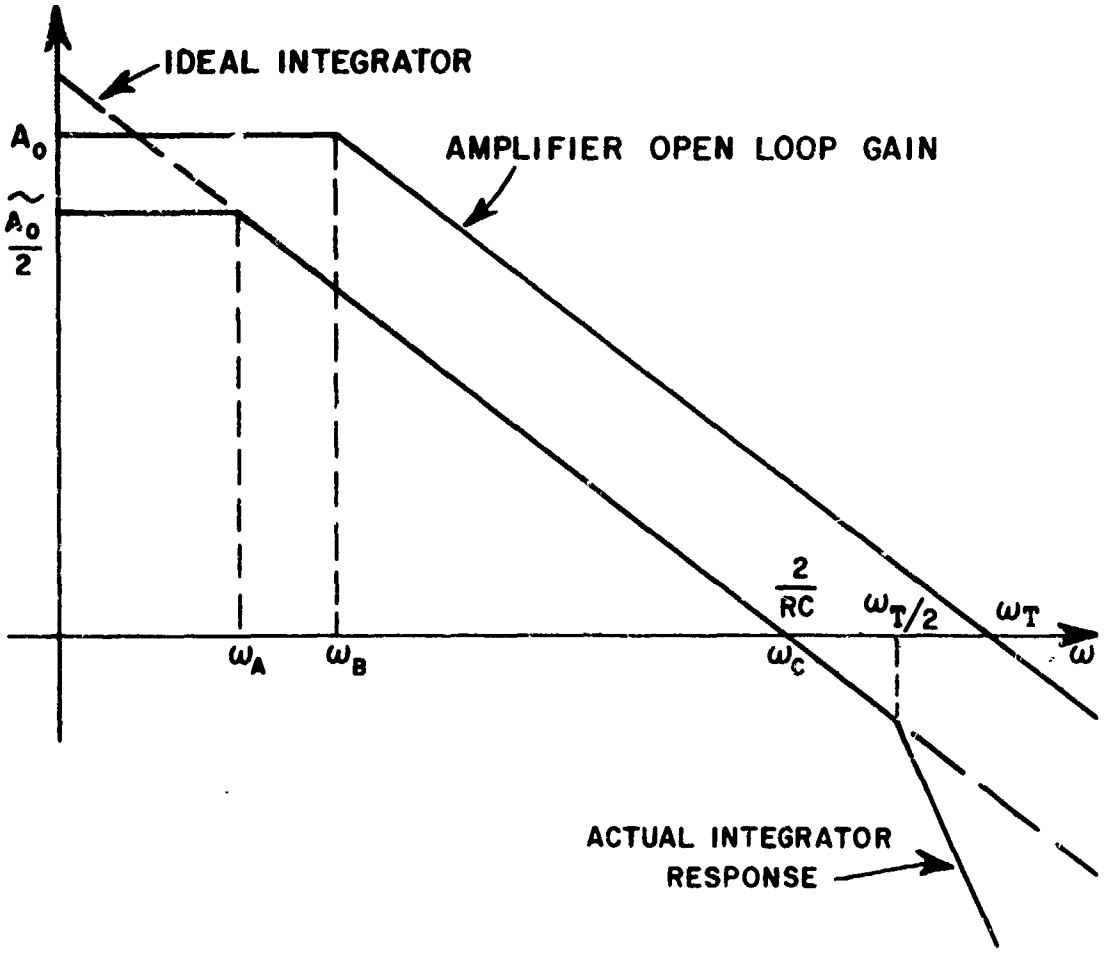

Fig. 33. Bode diagram comparing the transfer function of an ideal integrator to that of a practical integrator.

and

(124) $A_o >>> 1$,

then Eq. (121) can be approximated by[14]

$$(125) \qquad \frac{V_o}{V_i}(S) = \frac{1}{\frac{2}{A_o}\left(\frac{R}{R_o} + 1\right) + \frac{RC}{2}S + \frac{RC}{2\pi f_T}S^2} \quad .$$

A Bode diagram of the above expression, given in Fig. 33, shows that the practical integrator departs from an ideal integrator for large values of time and for small values of time.

For small values of time, $\pi R_o C f_T$ will normally be much less than the open loop gain A_o, but the relationship given in Eq. (123) may not hold if $\frac{2}{RC}$ approaches $\omega_T (= 2\pi f_T)$. Consequently, for a short integration period, $\frac{V_o}{V_i}(S)$ is approximated by

$$(126) \qquad \frac{V_o}{V_i}(S) = \frac{1}{S\left(\frac{RC}{2\pi f_T}S + \frac{1}{\pi f_T} + \frac{RC}{2}\right)} \quad .$$

The output voltage in response to an input step of amplitude E is given by

$$(127) \qquad V_o(t) = EF\left\{t + \tau_o\left[\exp(-\tau_o t) - 1\right]\right\} u(t)$$

where

$$(128) \qquad F = \frac{2\pi f_T}{2 + \pi RCf_T}$$

and

$$(129) \qquad \tau_o = \frac{RC}{2 + \pi RCf_T} \quad .$$

Equation (127) shows that the finite bandwidth f_T introduces a time lag equal to τ_o seconds at the integrator's output, as illustrated in Fig. 34. Also, if the constant $2(RC)^{-1}$ is of the same order of magnitude as ω_T, then the gain of the integrator will depend on f_T; this is usually undesirable because of temperature instabilities or parameter variations among op amps.

Substituting circuit parameters of the elements used in the DD integrate/dump circuit at the 50 Kbps rate, given by

$R = 2K\Omega$

$C = 0.002\ \mu f$

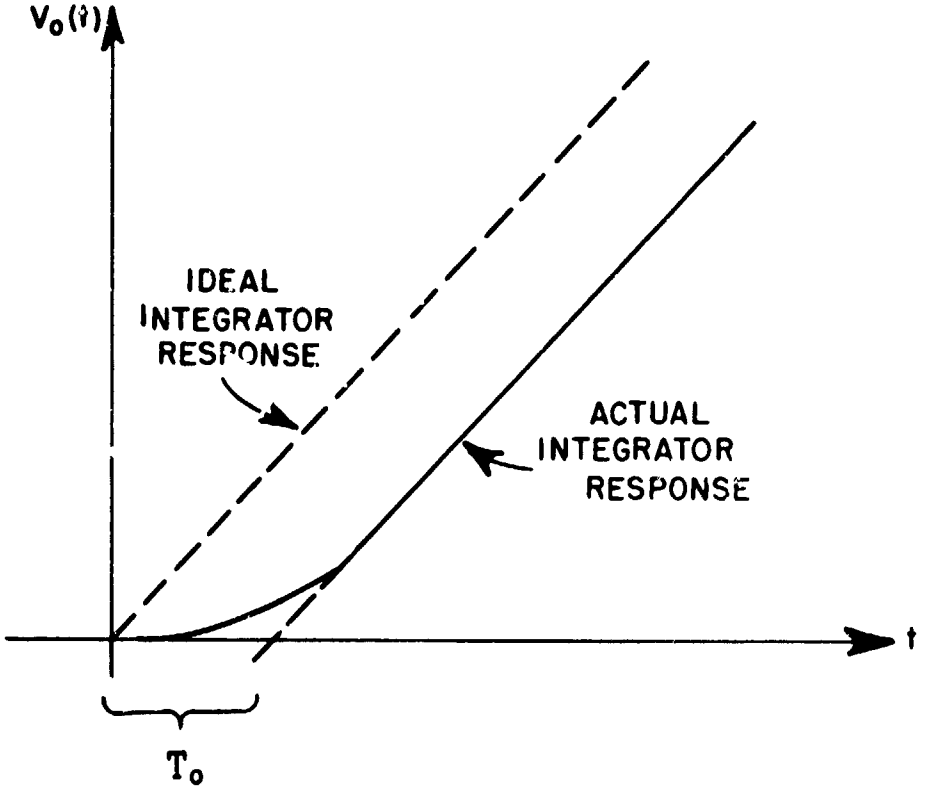

Fig. 34. The step response of an integrator for small values of time.

and

$$f_T = 10 \text{ MHz} \quad ,$$

into Eqs. (128) and (129), it is found that

(130) $\tau_o \doteq 31$ nsec

(131) $F \doteq 5 \times 10^5$

and

(132) $$G \equiv F \int_0^{T_b} dt = 5 \times 10^5 \int_0^{2 \times 10^{-5}} dt = 10 \quad .$$

At a 500 Kbps rate, with R, G, and f_T held constant, τ_o, C, and F are found to be

(133) $\tau_o \doteq 27$ nsec

(134) $C \doteq 168$ pf

and

(135) $F = 5 \times 10^6$.

The gain sensitivity to variations in f_T at the 500 Kbps rate,

(136) $$\frac{1}{F}\frac{dF}{df_T}\Bigg]_{f_T = 10 \text{ MHz}} = \frac{2}{f_T(2 + \pi R C f_T)}\Bigg]_{f_T = 10 \text{ MHz}} = 1.58\%/\text{MHz}$$

is, for most applications, acceptable.

The minimum dump time for the circuit of Fig. 32 is determined by 1) the turn-on time, $t_{d(on)}$, of the FET switch, 2) the on resistance, R_{on}, of the FET switch, 3) the value of the integrating capacitor (C), 4) the maximum acceptable intersymbol interference, and 5) the slew rate, S_r, of the operational amplifier. At the 50 Kbps rate, the circuit parameters were given by

$$R_{on} = 25\Omega$$

$$C = 0.002\,\mu f$$

$$S_r = 70\ V/\mu sec$$

$$t_{d(on)} = 6\ nsec \quad .$$

The dump interval was set so that the integrator's output voltage at the end of the dump interval equaled 0.002 times the output voltage at the beginning of the dump interval; correspondingly, at least 6.2 time constants must be spanned by the dump interval;

$$\delta_{MIN} = 6.2\,(R_{on}\,C) + t_{d(on)} = 316\ nsec \quad . \tag{137}$$

Since the worst case rise time* of the op amp is about 175 nsec, slew rate limiting does not need to be considered in this case. However, at the 500 Kbps rate,

*Here, worst case rise time is defined as the time required for the op amp to settle to within 0.002 times the full output voltage after the FET has turned on minus the delay τ_0.

(138) $6.2(R_{on}C) \triangleq 26$ nsec.

Consequently, the minimum dump time is limited by the slew rate to 175 nsec in this case. At either bit rate, the switching time of the J-FET is relatively small.

The dump time and the response for small values of time can be improved by using high speed op amps. For example, differential op amps with slew rates of 1000 V/μsec and f_T = 100 MHz are presently available; thus, the circuit given in Fig. 32 can provide acceptable performance for bit rates of 5 Mbps and above if appropriate devices are utilized.

B. The Sample/Hold Circuit

A schematic diagram of the sample/hold circuit is given in Fig. 35. It can be shown, in a manner similar to the analysis of the integrate/dump circuit, that the delay τ_o' of the output voltage in response to a ramp input is given by

(139) $\tau_o' = 120$ nsec.

The aperture time, defined as the sample to hold switching delay, was equal to about 20 nsec. Therefore, the total effective delay at the output of the sample/hold circuit, in response to a step at the integrator's input, is given by

(140) $D_o = \tau_o + \tau_o' + 20 \text{ nsec} = 171 \text{ nsec}$.

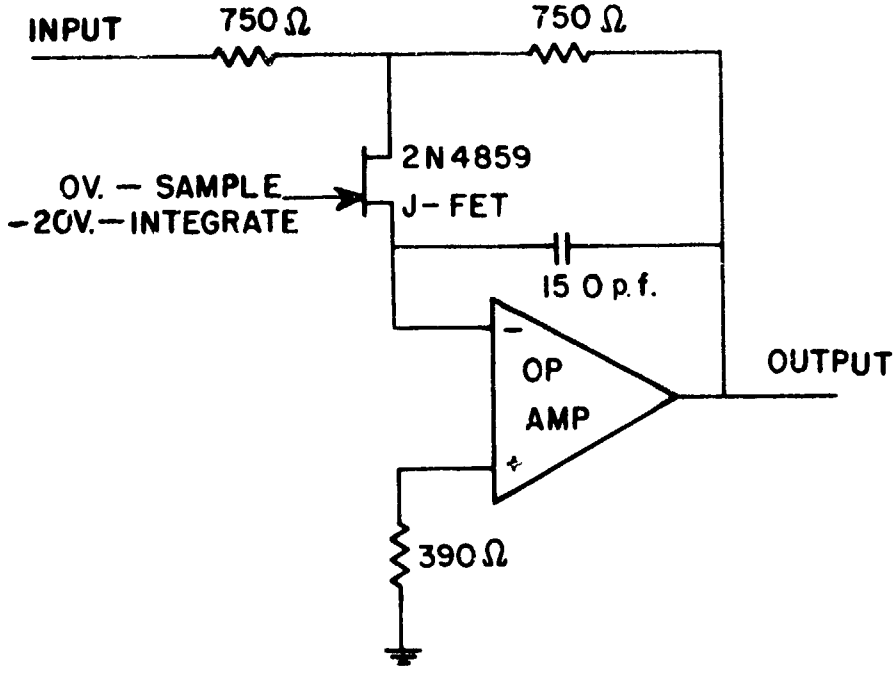

Fig. 35. A schematic diagram of the sample/hold circuit employed in the DD.

APPENDIX D
A LIST OF RECEIVER PARAMETERS

IF BANDWIDTH	2 MHz
DATA BIT RATE	50 Kbps
LO PHASE QUADRATURE ERROR	± 2°
DELAY AT S/H OUTPUT IN RESPONSE TO A STEP APPLIED AT THE INTEGRATOR'S INPUT	171 nsec
S/H APERATURE TIME	40 nsec
TOTAL MULTIPLIER ERROR	± 1% FULL SCALE
MULTIPLIER BANDWIDTH	3 MHz
DATA BIT RATE - DESIGN MAXIMUM	500 Kbps
ERROR IN MATCHING GAIN IN EACH ORTHOGONAL CHANNEL	$\pm \frac{1}{2}\%$

REFERENCES

1. Huff, R.J., "The Imperfectly-Timed Demodulation of Differential Phase Shift Keyed Signals," Report 2738-1, June 1969, ElectroScience Laboratory, Department of Electrical Engineering, The Ohio State University; prepared under Contract F30602-67-C-0112 for Rome Air Development Center, Griffiss Air Force Base, New York.

2. Huff, R.J., Reinhard, K.L., and Upp, D.C., "The Synchronization of Time Division Multiple Access Systems - An Analytical and Experimental Study," Report 2358-9, January 1969, ElectroScience Laboratory, Department of Electrical Engineering, The Ohio State University; prepared under Contract F30602-67-C-0119, Rome Air Development Center, Griffiss Air Force Base, New York.

3. Schwartz, J.W., Aein, J.M., and Kaiser, J., "Modulation Techniques for Multiple Access to a Hard-Limiting Satellite Repeater," Proc. IEEE, Vol. 54, (May 1966), pp. 763-777.

4. Masonson, M., UNICOM Progress Report for 7 and 8 Quarters, Vol. II, App. 58; January 1, 1961 - June 30, 1961. (unpublished).

5. Huff, R.J., "TDMA Space Communications System: Concepts and Practical Techniques," Report 2738-4, 13 August 1971, ElectroScience Laboratory, Department of Electrical Engineering, The Ohio State University; prepared under Contract F30602-67-C-0012 for Rome Air Development Center, Griffiss Air Force Base, New York.

6. Schwartz, M., Bennet, W.R., and Stein, S., Communications Systems and Techniques, New York, New York: McGraw-Hill, (1966), pp. 302-310.

7. Viterbi, A.J., Principles of Coherent Communications, New York, New York: McGraw-Hill, (1966), pp. 185-214.

8. Arthurs, E., and Dym, H., "On the Optimum Detection of Digital Signals in the Presence of White Gaussian Noise - A Geometrical Interpretation and a Study of Three Basic Data Transmission Systems," IRE Trans. on Communications Systems, Vol. CS-10, (December 1962), pp. 336-372.

9. Hancock, J.C., and Wintz, P.A., Signal Detection Theory, New York, New York: McGraw-Hill, (1966), pp. 156-167.

10. Henry, J.C., III, "DPSK versus FSK with Frequency Uncertainty," IEEE Trans. on Communications Technology, Vol. COM-18, (December 1970), pp. 814-817.

11. Salz, J. and Saltzberg, B.R., "Double Error Rates in Differentially Coherent Phase Systems," IEEE Trans. on Communications Systems, Vol. CS-12, (June 1964), pp. 202-205.

12. Papoulis, A., Probability, Random Variables, and Stochastic Processes, New York, New York: McGraw-Hill, (1965), pp. 235-237.

13. Natali, F.D. and Wolbesser, W.J., "Phase-Locked-Loop Detection of Binary PSK Signals Utilizing Decision Feedback," IEEE Trans. on Aerospace and Electronic Systems, Vol. AES-5, (January 1969), pp. 83-90.

14. Schick, L.L., "Linear Circuit Applications of Operational Amplifiers," IEEE Spectrum, Vol. 8, (April 1971), pp. 36-50.